

Mixed axion/neutralino cold dark matter in supersymmetric models

Howard Baer^a, Andre Lessa^a, Shibi Rajagopalan^{a,b} and Warintorn Sreethawong^a

^a*Dept. of Physics and Astronomy, University of Oklahoma, Norman, OK 73019, USA*

^b*Laboratoire de Physique Subatomique et de Cosmologie, UJF Grenoble 1,
CNRS/IN2P3, INPG, 53 Avenue des Martyrs, F-38026 Grenoble, France*

E-mail: baer@nhn.ou.edu, lessa@nhn.ou.edu, shibi@nhn.ou.edu, wstan@nhn.ou.edu

ABSTRACT: We consider supersymmetric (SUSY) models wherein the strong CP problem is solved by the Peccei-Quinn (PQ) mechanism with a concomitant axion/axino supermultiplet. We examine R -parity conserving models where the neutralino is the lightest SUSY particle, so that a mixture of neutralinos *and* axions serve as cold dark matter ($a\tilde{Z}_1$ CDM). The mixed $a\tilde{Z}_1$ CDM scenario can match the measured dark matter abundance for SUSY models which typically give too low a value of the usual thermal neutralino abundance, such as models with wino-like or higgsino-like dark matter. The usual thermal neutralino abundance can be greatly enhanced by the decay of thermally-produced axinos (\tilde{a}) to neutralinos, followed by neutralino re-annihilation at temperatures much lower than freeze-out. In this case, the relic density is usually neutralino dominated, and goes as $\sim (f_a/N)/m_a^{3/2}$. If axino decay occurs before neutralino freeze-out, then instead the neutralino abundance can be augmented by relic axions to match the measured abundance. Entropy production from late-time axino decays can diminish the axion abundance, but ultimately not the neutralino abundance. In $a\tilde{Z}_1$ CDM models, it may be possible to detect both a WIMP and an axion as dark matter relics. We also discuss possible modifications of our results due to production and decay of saxions. In the appendices, we present expressions for the Hubble expansion rate and the axion and neutralino relic densities in radiation, matter and decaying-particle dominated universes.

KEYWORDS: Supersymmetry Phenomenology, Supersymmetric Standard Model, Dark Matter, Axions.

1. Introduction

The Standard Model of particle physics is beset by two major fine-tuning problems. The first occurs in the Higgs sector of the electroweak model, where quantum corrections to the Higgs mass push m_h up to the energy scale associated with the cut-off of the theory, where new physics is expected to enter. The electroweak fine-tuning problem is elegantly solved by the introduction of weak scale supersymmetry (SUSY)[1]. A consequence of weak scale SUSY is that supersymmetric matter states should exist at or around the electroweak scale, and ought to be detectable at the CERN LHC[2].

The second fine-tuning problem arises in the QCD sector. Here, t’Hooft’s solution to the $U(1)_A$ problem[3] via instantons and the θ vacuum requires the existence of a CP violating term

$$\mathcal{L}_\theta = \frac{\theta}{32\pi^2} F_{A\mu\nu} \tilde{F}_A^{\mu\nu} \quad (1.1)$$

in the QCD Lagrangian[4]. A second contribution to \mathcal{L}_θ arises from the electroweak sector, and is proportional to $\arg(\det\mathcal{M})$, where \mathcal{M} is the quark mass matrix[5]. Measurements of the neutron EDM tell us that the combination $\theta + \arg(\det\mathcal{M}) \equiv \bar{\theta}$ must be $\lesssim 10^{-11}$ [6]. Explaining why $\bar{\theta}$ is so small is known as the strong CP problem. The strong CP problem is elegantly solved by the Peccei-Quinn mechanism[7] and its concomitant *axion* a [8]. Models of an “invisible axion” with PQ breaking scale $f_a/N \gtrsim 10^9$ GeV (with N being the color anomaly factor, which is 1 for KSZV[9] models and 6 for DFSZ[10] models) allow for a solution to the strong CP problem while eluding astrophysical constraints arising due to energy loss from stars in the form of axion radiation[11].

Of course, the SUSY solution to the electroweak fine-tuning, and the PQ solution to the strong fine-tuning are not mutually exclusive. In fact, each complements the other[12], and both are expected to arise rather naturally from superstring models[13]. In models which invoke both R -parity conserving SUSY and the PQ solution to the strong CP problem, the dark matter of the universe is expected to consist of a *mixture* of both the axion and the lightest-SUSY-particle (LSP). Many previous studies have focused on the possibility of an axino \tilde{a} as the LSP[14, 15, 16], giving rise to mixed axion/axino cold dark matter (CDM)[17]. In this paper, we explore instead the possibility that the lightest neutralino \tilde{Z}_1 is the LSP, thus giving rise to mixed axion/neutralino ($a\tilde{Z}_1$) CDM. In the case of mixed $a\tilde{Z}_1$ CDM, it may be possible to detect relic axions as well as relic neutralinos (as WIMPs).

The case of neutralino CDM in the PQ-augmented MSSM has been considered previously by Choi *et al.*[18]. In Ref. [18], the authors considered the case of neutralino dark matter where $m_{\tilde{a}} > m_{\tilde{Z}_1}$. They presented approximate expressions to estimate the relic density of neutralinos $\Omega_{\tilde{Z}_1} h^2$. They found that neutralinos can be produced thermally as usual, but also that their abundance can be *augmented* by thermal production of axinos in the early universe, followed by axino cascade decays into the stable \tilde{Z}_1 state. However, the neutralino abundance could also be *diminished* by two effects. The first is that even after neutralino freeze-out, the additional late-time injection of neutralinos into the cosmic soup from axino decay can cause a re-annihilation effect. The second diminution effect occurs

when late decaying axinos inject entropy into the early universe after neutralino freeze-out, thus possibly diluting the frozen-out neutralino abundance.

In this paper, our goal is to present explicit numerical calculations of the relic abundance of mixed $a\tilde{Z}_1$ CDM in SUSY models. To this end, we include several new effects.

- First, we note that in the PQMSSM with a \tilde{Z}_1 as LSP, the dark matter will consist of an axion/neutralino admixture, so we always account for the axion contribution to the total DM abundance.
- Second, we account for the measured abundance of CDM as is given by the recent WMAP7 analysis[19]:

$$\Omega_{\text{DM}}h^2 = 0.1123 \pm 0.0035 \quad \text{at 68\% CL.} \quad (1.2)$$

We seek to establish under what conditions of model parameters the theoretical prediction for the relic abundance of mixed $a\tilde{Z}_1$ CDM can be in accord with the measured value.

- Third, we seek to establish whether, when fulfilling the WMAP measured abundance, the mixed $a\tilde{Z}_1$ DM is dominantly axion or dominantly neutralino, or a comparable mixture. Such an evaluation is important for determining the relative prospects of axion and WIMP direct detection experiments.

The remainder of this paper is organized as follows. In Sec. 2, we introduce two SUSY benchmark models— the first from the minimal supergravity (mSUGRA) model[20] in the hyperbolic branch/focus point region[21] (where neutralinos are expected to be of the mixed higgsino variety) and the second arising from the gaugino AMSB[22] model[23, 24] (where the neutralino is of the nearly pure wino variety). These benchmarks will be used for illustrative calculations of mixed $a\tilde{Z}_1$ CDM. In Sec. 3, we calculate the axino decay rate into all possible modes, while in Sec. 4 we discuss the thermal production of axinos in the early universe. In Sec. 5, we compute the temperature T_D at which axinos decay, and the temperature T_e at which they might dominate the energy density of the universe. In Sec. 6 and in Sec. 7, we discuss the computation of the axion and the neutralino relic density. In the case of neutralino production, we pay special attention to the neutralino re-annihilation which takes place due to injection of neutralinos into the early universe from axino decay. In Sec. 8 we present our algorithm for estimating the mixed $a\tilde{Z}_1$ CDM abundance in SUSY models. In Sec. 9, we present our numerical results, and in Sec. 10 we discuss the effect of including saxion production and decay in the calculation. In Sec. 11, we present our conclusions. In the appendices, we present explicit formulae for the Hubble expansion rate, the axion abundance, and the thermal neutralino abundance for a universe that is either radiation-dominated (RD), matter-dominated (MD), or decaying-particle-dominated (DD).

2. Two benchmark scenarios

Supersymmetric models with mixed $a\tilde{Z}_1$ CDM will always have a neutralino dark matter component, which is mainly enhanced by axino production and decay, but might also be

diminished by further annihilations and by entropy injection. In addition, there will always be an axion component to the CDM, which arises as usual via vacuum misalignment. In SUGRA-based models with gaugino mass unification, the lightest neutralino \tilde{Z}_1 is usually bino-like, and annihilation reactions are suppressed by their p -wave annihilation cross sections, leading to an overabundance of neutralinos[25]. Since SUSY models with mixed $a\tilde{Z}_1$ CDM will have to crowd both \tilde{Z}_1 s and axions into the overall relic density, we find that the most promising models to realize mixed $a\tilde{Z}_1$ CDM are those leading to an *underabundance* of the usual calculation of thermally-produced neutralinos, such as models with either a higgsino-like or wino-like \tilde{Z}_1 state[26]: such neutralinos annihilate via s -wave rather than p -wave reactions, and naively suffer a *dearth* of relic abundance.

We will thus choose two benchmark cases to examine mixed $a\tilde{Z}_1$ CDM. The first occurs in the hyperbolic branch/focus point region[21] of mSUGRA[20] and has a mixed higgsino-wino-bino \tilde{Z}_1 state, while the second is taken from the gaugino-anomaly-mediated-SUSY-breaking model (inoAMSB)[24], which leads to a nearly pure wino-like \tilde{Z}_1 state.

2.1 Mixed higgsino DM in HB/FP region of mSUGRA model

The spectra for our first benchmark model, BM1, is generated within the minimal supergravity, or mSUGRA model, using the Isasugra[27] spectrum generator from Isajet v7.81[28]. The input parameters are taken as

- $(m_0, m_{1/2}, A_0, \tan\beta, \text{sign}(\mu) = (4525 \text{ GeV}, 275 \text{ GeV}, 0, 10, +)$

with $m_t = 173.3 \text{ GeV}$. The \tilde{Z}_1 has mass 87.9 GeV, while the calculated thermal abundance of neutralinos from IsaReD[29] is $\Omega_{\tilde{Z}_1}^{std} h^2 = 0.05$. Many sparticle masses and low energy observables are listed in Table 1. Since the weak scale value of the superpotential μ term is only 137.2 GeV, the \tilde{Z}_1 is of mixed higgsino-bino-wino type.

2.2 Wino-like DM from gaugino AMSB

The spectra for benchmark point BM2 of Table 1 is generated within the gaugino AMSB model which is expected to arise in string theories with moduli-stabilization via fluxes and a large volume compactification[23]. In the inoAMSB model, the parameters are taken as

- $m_{3/2}, \tan\beta, \text{sign}(\mu) = (50 \text{ TeV}, 10, +)$

while $m_0 = A_0 = 0$ at the GUT scale. The GUT scale gaugino masses take the AMSB form, and are given at m_{GUT} as $M_1 = 1065.3 \text{ GeV}$, $M_2 = 161.4 \text{ GeV}$ and $M_3 = -484 \text{ GeV}$. This choice leads to a neutralino state \tilde{Z}_1 which is nearly pure wino, with a thermal relic abundance of $\Omega_{\tilde{Z}_1}^{std} h^2 = 0.0016$ as indicated in Table 1.

3. Axino decays in the mixed axion-neutralino CDM scenario

Since we assume $m_{\tilde{a}} > m_{\tilde{Z}_1}$, an important element in the thermal history of the universe with mixed $a\tilde{Z}_1$ CDM will be knowledge of the axino decay width.

	BM1 (HB/FP)	BM2 (inoAMSB)
m_0	4525	0
$m_{1/2}$	275	–
A_0	0	0
$\tan \beta$	10	10
$m_{3/2}$ [TeV]	–	50
μ	137.2	599.4
$m_{\tilde{g}}$	810.4	1129.7
$m_{\tilde{u}_L}$	4517.0	993.9
$m_{\tilde{t}_1}$	2608.1	861.4
$m_{\tilde{b}_1}$	3687.6	926.1
$m_{\tilde{e}_L}$	4520.1	229.4
$m_{\tilde{W}_1}$	121.1	142.4
$m_{\tilde{Z}_4}$	273.4	616.3
$m_{\tilde{Z}_3}$	149.8	606.0
$m_{\tilde{Z}_2}$	143.1	443.6
$m_{\tilde{Z}_1}$	87.9	142.1
m_A	4458.1	633.6
m_h	119.6	112.1
$v_4^{(1)}$	0.65	0.01
$\Omega_{\tilde{Z}_1}^{std} h^2$	0.05	0.0016
T_{fr}	$m_{\tilde{Z}_1}/23.2$	$m_{\tilde{Z}_1}/31.2$
$\langle \sigma v \rangle$ [GeV $^{-2}$]	4.3×10^{-9}	1.8×10^{-7}
$\sigma(\tilde{Z}_1 p)$ [pb]	3.2×10^{-8}	4.3×10^{-9}

Table 1: Masses and parameters in GeV units for the HB/FP and inoAMSB benchmark points. computed with ISAJET 7.81 using $m_t = 173.3$ GeV.

The axino-gluon-gluino coupling is given by

$$\mathcal{L}_{\tilde{a}\tilde{g}g} = i \frac{\alpha_s}{16\pi(f_a/N)} \tilde{a} \gamma_5 [\gamma^\mu, \gamma^\nu] \tilde{g}_A F_{A\mu\nu}. \quad (3.1)$$

Evaluation of the $\tilde{a} \rightarrow g\tilde{g}$ decay width gives a result in accord with Ref. [18], and is given by

$$\Gamma(\tilde{a} \rightarrow g\tilde{g}) = \frac{8\alpha_s^2}{128\pi^3(f_a/N)^2} m_{\tilde{a}}^3 \left(1 - \frac{m_{\tilde{g}}^2}{m_{\tilde{a}}^2}\right)^3. \quad (3.2)$$

Also, the axino-bino- B_μ coupling is given by

$$\mathcal{L}_{\tilde{a}\tilde{B}B} = i \frac{\alpha_Y C_{aYY}}{16\pi(f_a/N)} \tilde{a} \gamma_5 [\gamma^\mu, \gamma^\nu] \tilde{B} B_{\mu\nu}, \quad (3.3)$$

where $\alpha_Y = g'^2/4\pi$, $B_{\mu\nu} = \partial_\mu B_\nu - \partial_\nu B_\mu$ and C_{aYY} is a model-dependent factor equal to 8/3 in the DFSZ model, and 0, 2/3, 8/3 for heavy quark charges $e_Q = 0, -1/3, +2/3$ in

the KSVZ model. For numerical purposes, we will take $C_{aYY} = 8/3$ since that case occurs in both models. We then find:

$$\Gamma(\tilde{a} \rightarrow \tilde{Z}_i + \gamma) = \frac{\alpha_Y^2 C_{aYY}^2 \cos^2 \theta_w v_4^{(i)2}}{128\pi^3 (f_a/N)^2} m_{\tilde{a}}^3 \left(1 - \frac{m_{\tilde{Z}_i}^2}{m_{\tilde{a}}^2}\right)^3 \quad (3.4)$$

and

$$\Gamma(\tilde{a} \rightarrow \tilde{Z}_i + Z) = \frac{\alpha_Y^2 C_{aYY}^2 \sin^2 \theta_w v_4^{(i)2}}{128\pi^3 (f_a/N)^2} m_{\tilde{a}}^3 \lambda^{1/2} \left(1, \frac{m_{\tilde{Z}_i}^2}{m_{\tilde{a}}^2}, \frac{m_Z^2}{m_{\tilde{a}}^2}\right) \cdot \left\{ \left(1 - \frac{m_{\tilde{Z}_i}^2}{m_{\tilde{a}}^2}\right)^2 + 3 \frac{m_{\tilde{Z}_i} m_Z^2}{m_{\tilde{a}}^3} - \frac{m_Z^2}{2m_{\tilde{a}}^2} \left(1 + \frac{m_{\tilde{Z}_i}^2}{m_{\tilde{a}}^2} + \frac{m_Z^2}{m_{\tilde{a}}^2}\right) \right\}, \quad (3.5)$$

where $v_4^{(i)}$ is the bino fraction of \tilde{Z}_i in the notation of Ref. [1].

The axino partial and total widths are exhibited in Fig. 1 for *a*). the HB/FP model and *b*). the inoAMSB model. We see that at very low values of $m_{\tilde{a}} \sim m_{\tilde{Z}_1}$, only the decay $\tilde{a} \rightarrow \tilde{Z}_1 \gamma$ is open, and $\Gamma_{\tilde{a}}$ is very small. As $m_{\tilde{a}}$ increases, additional decay modes become allowed, and contribute to $\Gamma_{\tilde{a}}$. In frame *b*)., $\Gamma_{\tilde{a}}$ enjoys a large increase when the decay to $\tilde{Z}_2 \gamma$ opens up, since in the inoAMSB case, the \tilde{Z}_2 is mainly bino-like. Once the decay to $\tilde{g} g$ opens up, this mode is dominant. Decays to $\tilde{Z}_i Z$ are always subdominant to $\tilde{Z}_i \gamma$, owing to the fact that the photon has a larger B_μ component than does the Z .

4. Thermal production of axinos in the early universe

If the reheat temperature after inflation, T_R , exceeds the axino decoupling temperature[14],

$$T_{dcp} = 10^{11} \text{ GeV} \left(\frac{f_a/N}{10^{12} \text{ GeV}} \right)^2 \left(\frac{0.1}{\alpha_s} \right)^3, \quad (4.1)$$

then reheat occurred before decoupling which allowed the axinos to reach thermal equilibrium. Their number density at the time of decoupling is given in terms of the yield variable, $Y \equiv n/s$, as

$$Y_{\tilde{a}} = \frac{n_{\tilde{a}}}{s}|_{T_{dcp}} = \frac{135\zeta(3)}{4\pi^4} \frac{1}{g_*(T_{dcp})}, \quad (4.2)$$

with $\zeta(3) \simeq 1.202$, $g_*(T_{dcp})$ is the effective number of relativistic degrees of freedom at temperature T_{dcp} , and $s = \frac{2\pi^2}{45} g_* T^3$ is the entropy density of radiation¹.

In the other case, where $T_R < T_{dcp}$, the axinos were never in thermal equilibrium in the early universe. However, they could still be produced thermally via radiation off of other particles in thermal equilibrium [15, 30]. Here, we adopt a recent calculation of the thermally produced axino yield from Strumia [31]:

$$Y_{\tilde{a}}^{\text{TP}} = 4.5 \times 10^{-9} g_s^4 F(g_s) \frac{T_R}{10^4 \text{ GeV}} \left(\frac{10^{11}}{f_a/N} \right)^2, \quad (4.3)$$

¹For simplicity we assume $g_{*S}(T) = g_*(T)$, where g_{*S} is the total number of relativistic degrees of freedom at T used to compute s .

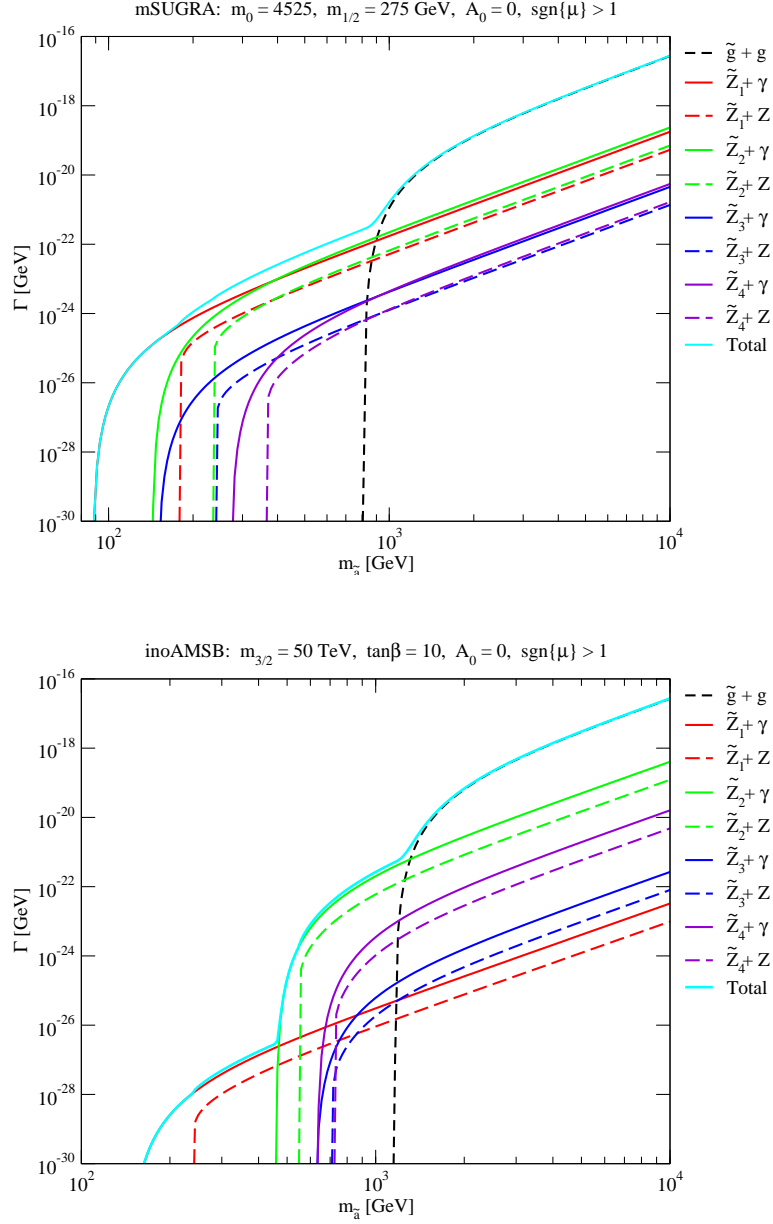


Figure 1: Partial and total decay width of axinos versus $m_{\tilde{a}}$ for BM1 in the mSUGRA model with $(m_0, m_{1/2}, A_0, \tan \beta, \text{sign}(\mu)) = (4525, 275, 0, 10, +)$ and for BM2 in the inoAMSB model with $m_{3/2} = 50$ TeV, $\tan \beta = 10$ and $\mu > 0$. We take $f_a/N = 10^{12}$ GeV.

with $F(g_s) \sim 20g_s^2 \ln \frac{3}{g_s}$, and g_s is the strong coupling constant evaluated at $Q = T_R$.

If we suppose that each produced axino will cascade decay into the \tilde{Z}_1 state, we can naively estimate the decay-induced neutralino abundance by

$$\Omega_{\tilde{Z}_1}^{\tilde{a}} h^2 = \frac{m_{\tilde{Z}_1}}{m_{\tilde{a}}} \Omega_{\tilde{a}}^{TP} h^2. \quad (4.4)$$

This estimate of the neutralino abundance from the decay of thermally-produced axinos is

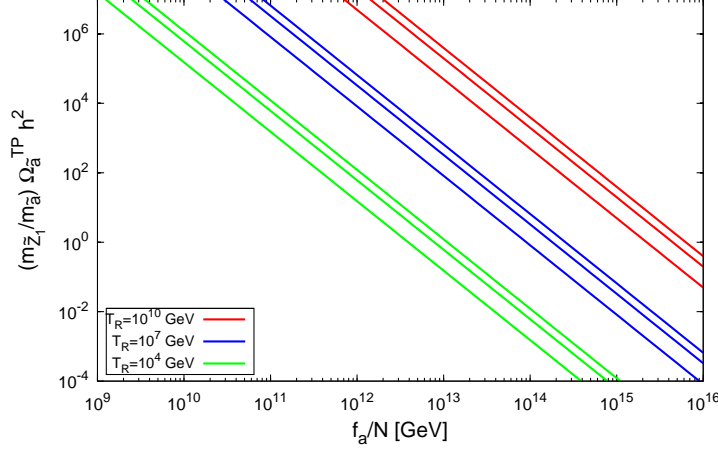


Figure 2: Plot of $\Omega_{\tilde{Z}_1}^{\tilde{a}} h^2$ versus f_a/N for various values of T_R and $m_{\tilde{Z}_1} = 50, 200$ and 400 GeV (lower-to-upper).

shown in Fig. 2 as a function of f_a/N for $T_R = 10^4, 10^7$ and 10^{10} GeV (green, blue and red curves, respectively), and for $m_{\tilde{Z}_1} = 50, 200$ and 400 GeV (lower to upper curves). We see that the neutralino relic density from axino decay can be enormous, and it typically dominates over the thermal neutralino abundance as calculated, for instance, from the mSUGRA model. From our naive estimate, we see that a tremendous overproduction of neutralinos is obtained from thermal axino production and decay except when considering parameter regions of high f_a/N or low T_R where the axino production rate is suppressed.

5. Axino domination of the Universe

Once the decay width of the axino has been calculated as in Sec. 3, we may then calculate the axino lifetime or, alternatively, the temperature of radiation at the time scale when nearly all axinos have decayed, T_D . This is achieved by equating the Hubble and the decay rates

$$H(T_D) = \Gamma_{\tilde{a}}, \quad (5.1)$$

which implies

$$T_D = \sqrt{\Gamma_{\tilde{a}} M_P / (\pi^2 g_*(T_D)/90)}^{1/4}, \quad (5.2)$$

where M_P is the reduced Planck mass $M_P \simeq 2.4 \times 10^{18}$ GeV. The temperature T_D also corresponds to the temperature of radiation when entropy injection from axino decays is nearly finished. We assume an exponential decay law for \tilde{a} which implies that the axino decays only cause a slow-down in the rate of cooling of the expanding universe[32]. In this case, T_D should not be interpreted as a “second reheat” temperature.

As the universe—filled with axinos and radiation—expands and cools, T drops below $m_{\tilde{a}}$ and the axinos become non-relativistic. At that point, the axino energy density decreases as T^3 , while the radiation energy density continues to decrease faster as T^4 . At some

temperature T_e , the energy density of axinos will dominate the universe if the axinos have not yet decayed, *i.e.* provided $T_e > T_D$. By equating the energy density of radiation $\rho_R = \pi^2 g_* T^4/30$ with the energy density of axinos $\rho_{\tilde{a}}|_{T < m_{\tilde{a}}} = m_{\tilde{a}} Y_{\tilde{a}} s$, we can determine T_e to be [18]

$$T_e = \frac{4}{3} m_{\tilde{a}} Y_{\tilde{a}}. \quad (5.3)$$

Furthermore, we can estimate the ratio of entropy after to the entropy before axino decay, r , again where $T_e > T_D$, by [32]

$$r = \frac{S_f}{S_0} \simeq \frac{4 m_{\tilde{a}} Y_{\tilde{a}}}{3 T_D} = T_e / T_D. \quad (5.4)$$

In Fig. 3a), we plot the values of T_D , T_e and the temperature of neutralino freeze-out T_{fr} versus $m_{\tilde{a}}$ for the benchmark BM1: the HB/FP region of the mSUGRA model. We take $f_a/N = 10^{12}$ GeV, and show T_e for $T_R = 10^6$ and 10^{10} GeV. For values of $T_D \lesssim 2$ MeV (gray shaded region), the parameters would be likely excluded because axinos would dump entropy after BBN has started. For $T_D > T_{fr}$ —the high $m_{\tilde{a}}$ region—axinos decay to neutralinos before freeze-out. In this case, the neutralinos from axino decays thermalize and the neutralino relic abundance $\Omega_{\tilde{Z}_1} h^2$ is given as usual by the standard calculation of WIMP thermal abundance ($\Omega_{\tilde{Z}_1}^0 h^2$). The region where $T_e > T_D$ is where axinos can dominate the universe. This occurs for $m_{\tilde{a}} \lesssim 8$ TeV in the $T_R = 10^{10}$ GeV case. Furthermore, the ratio between the T_e and T_D curves gives an approximate measure of the entropy injection from axino decay. In frame a). for $T_R = 10^6$ GeV, axinos never dominate the universe, since they decay prior to the point where the axino energy density exceeds that of radiation.

In frame b). of Fig. 3, we show the same temperatures, but this time for BM2, the inoAMSB case with wino dark matter. In this case, the region with $m_{\tilde{a}} \lesssim 550$ GeV is excluded by BBN constraints since the axino width is suppressed by the fact that only the decay to $\tilde{Z}_1 \gamma$ is open, where the bino component of \tilde{Z}_1 is tiny. When the decay $\tilde{a} \rightarrow \tilde{Z}_2 \gamma$ turns on around $m_{\tilde{a}} \sim 450$ GeV, the axino width rapidly increases, and the heavy axino scenario becomes BBN-allowed. For $T_R = 10^{10}$ GeV, axino domination occurs out to $m_{\tilde{a}} \sim 10$ TeV, while for higher $m_{\tilde{a}}$ values, the axino decays before neutralino freeze-out. For the $T_R = 10^6$ GeV case, axino domination only occurs in the BBN excluded region.

In order to see how large the increase in entropy due to axino decay can be, we plot in Fig. 4 regions of r ranging in value from 1 to $> 10^4$ in the f_a/N vs. T_R plane for $m_{\tilde{a}} = 1$ TeV and a). the BM1 benchmark and b). the BM2 benchmark. The region with $f_a/N \gtrsim 10^{13}$ GeV is likely BBN excluded since the axino decay temperature T_D drops below ~ 2 MeV. From Fig. 4, we see that when $T_R < T_{dcp}$, and axinos are produced via Eq. 4.3, r decreases with increasing f_a/N . Also, r increases with increasing T_R due to enhanced thermal production of axinos. In contrast, when $T_R > T_{dcp}$, the axinos are produced in thermal equilibrium and the production rate is independent of f_a/N . In this case, the r contours increase with increasing f_a/N , while they are also independent of T_R .

6. Axion production from vacuum misalignment

As already mentioned, the axion will contribute to the total dark matter, so we wish to

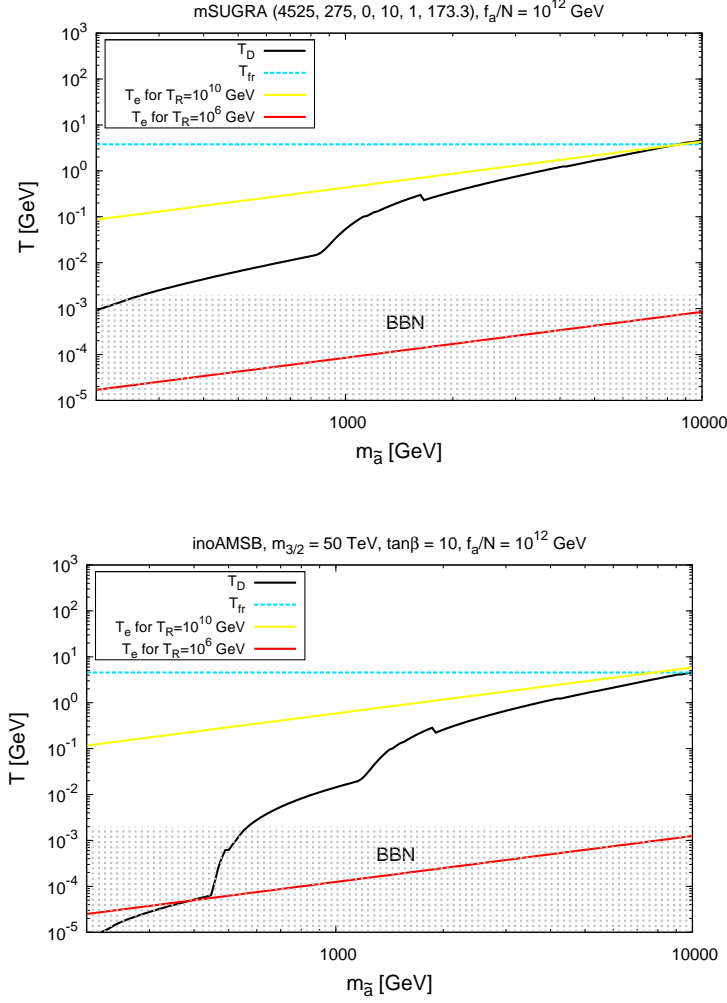


Figure 3: Plot of T_D , T_e and T_{fr} versus $m_{\tilde{a}}$ in the BM1 and BM2 benchmark models with $f_a/N = 10^{12}$ GeV.

review how it is produced. We consider the scenario where the PQ symmetry breaks before the end of inflation, so that a nearly uniform value of the axion field $\theta_i \equiv a(x)/(f_a/N)$ is expected throughout the universe. As implied by its equation of motion, the axion field stays relatively constant until temperatures approach the QCD scale $T_{QCD} \sim 1$ GeV. At this point, a temperature-dependent axion mass term turns on, and a potential is induced for the axion field. At temperature T_a the axion field begins to oscillate, filling the universe with low energy (cold) axions. The standard axion relic density (via this vacuum mis-alignment mechanism) is derived assuming that coherent oscillations begin in a radiation-dominated (RD) universe ($T_a < T_D$ or $T_a > T_e$), and its final form is given by [33, 34]

$$\Omega_a^{std} h^2 \simeq 0.23 f(\theta_i) \theta_i^2 \left(\frac{f_a/N}{10^{12} \text{ GeV}} \right)^{7/6} \quad (6.1)$$

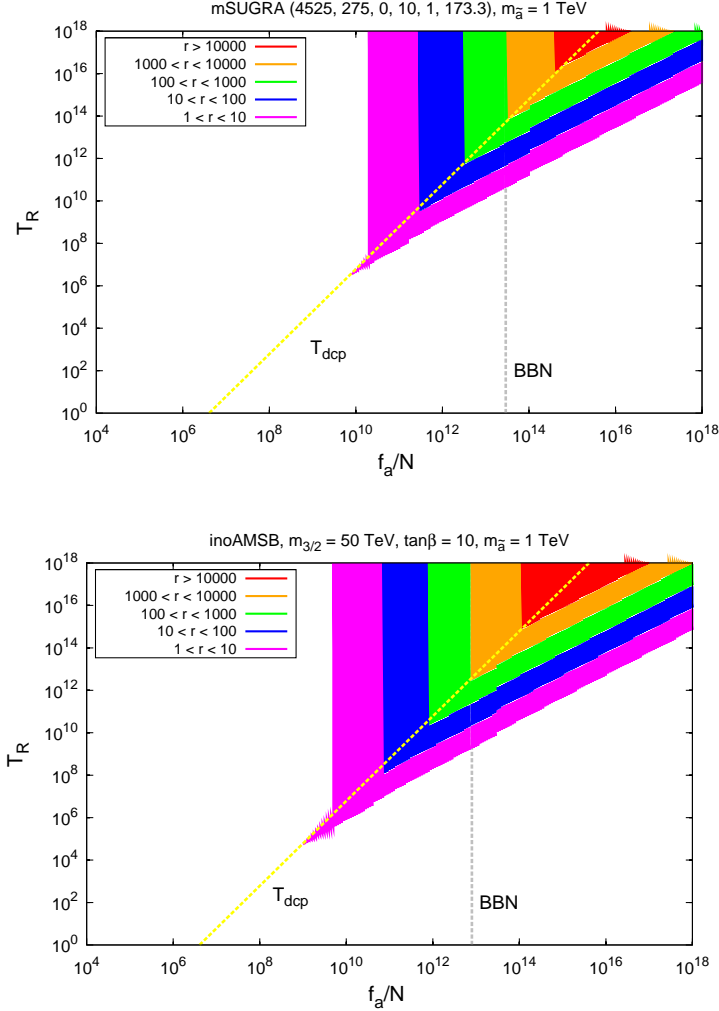


Figure 4: Plot of r values in the f_a/N vs. T_R plane for a) the FP model and b) the inoAMSB model, with $m_{\tilde{a}} = 1$ TeV.

where $0 < \theta_i < \pi$ and $f(\theta_i)$ is the anharmonicity factor. Visinelli and Gondolo [34] parametrize the latter as $f(\theta_i) = \left[\ln \left(\frac{e}{1 - \theta_i^2/\pi^2} \right) \right]^{7/6}$. The uncertainty in $\Omega_a h^2$ from vacuum mis-alignment is estimated as plus-or-minus a factor of three.

However, if the axion oscillation starts during the matter dominated (MD) or the decaying particle dominated (DD) phase ($T_D < T_a < T_e$), the axion relic density will no longer be given by Eq. 6.1. The appropriate expressions for each of these cases are given in Appendix B.

7. Relic abundance of neutralinos

In Ref. [18], formulae for the relic abundance of neutralinos are derived which include the effects of enhancement from axino production and decay and diminution from the

re-annihilation effect and entropy dilution. The starting point to evaluate the neutralino abundance is the Boltzmann equation

$$\frac{dn_{\tilde{Z}_1}}{dt} + 3Hn_{\tilde{Z}_1} = -\langle\sigma v\rangle n_{\tilde{Z}_1}^2, \quad (7.1)$$

where $n_{\tilde{Z}_1}$ is the neutralino number density, $H(t)$ is the Hubble constant at time t ($H^2 = \rho(t)/3M_P^2$), σ is the neutralino annihilation cross section, v is the $\tilde{Z}_1 - \tilde{Z}_1$ relative velocity and $\langle\cdots\rangle$ denotes thermal averaging. At very early times and high temperatures, $n_{\tilde{Z}_1}$ is given by the thermal equilibrium abundance, but as the universe expands and cools, at a temperature T_{fr} the expansion rate H outstrips the annihilation rate $n_{\tilde{Z}_1}\langle\sigma v\rangle$, and a relic abundance of neutralinos freezes out. Thus, we define here the freeze-out temperature by the value of T at which

$$\langle\sigma v\rangle n_{\tilde{Z}_1} \simeq H(T_{fr}). \quad (7.2)$$

From this condition we can compute the yield variable $Y = n_{\tilde{Z}_1}/s$:

$$Y_{\tilde{Z}_1}^{fr}(T_{fr}) = k_{fr} \times \frac{n_{\tilde{Z}_1}}{s} = \frac{H(T_{fr})}{\langle\sigma v\rangle s}. \quad (7.3)$$

where $k_{fr} = 1(3/2)$ if the freeze-out happens in the radiation (matter) dominated phase. If we assume a nearly constant value of $\langle\sigma v\rangle$ (which is appropriate for a higgsino- or wino-like \tilde{Z}_1 which dominantly annihilates via s -wave reactions), and freeze-out in a radiation-dominated universe with $H^2 = \rho_{rad}/3M_P^2$ and $\rho_{rad} = \pi^2 g_* T^4/30$, then one obtains

$$Y_{\tilde{Z}_1}^{fr} = \frac{(90/\pi^2 g_*(T_{fr}))^{1/2}}{4\langle\sigma v\rangle M_P T_{fr}}. \quad (7.4)$$

The usual cosmological assumption is that the yield $Y_{\tilde{Z}_1}^{fr}$ is conserved from $T = T_{fr}$ to T_0 , where T_0 is the present day temperature of radiation $T_0 = 2.725^\circ\text{K}$. In this case the thermal neutralino relic density is simply

$$\Omega_{\tilde{Z}_1}^{fr} h^2 = \frac{2\pi^2}{45} \frac{g_*(T_0) T_0^3}{\rho_c/h^2} m_{\tilde{Z}_1} Y_{\tilde{Z}_1}^{fr} \quad (7.5)$$

However, just as in the axion case, we must re-evaluate $Y_{\tilde{Z}_1}^{fr}$ at $T = T_D$, and also the freeze-out temperature, in the cases of a MD or a DD universe. The various yield expressions are contained in Appendix C.

7.1 Neutralino re-annihilation at $T = T_D$

In the mixed $a\tilde{Z}_1$ DM scenario, neutralinos are produced via axino decay at temperature $T = T_D$, as well as via thermal freeze-out at $T = T_{fr}$. The needed condition for re-annihilation at $T \sim T_D$ is that the annihilation rate exceeds the expansion rate at $T = T_D$:

$$\langle\sigma v\rangle \frac{n_{\tilde{Z}_1}(T_D)}{s} > \frac{H(T_D)}{s} \quad (7.6)$$

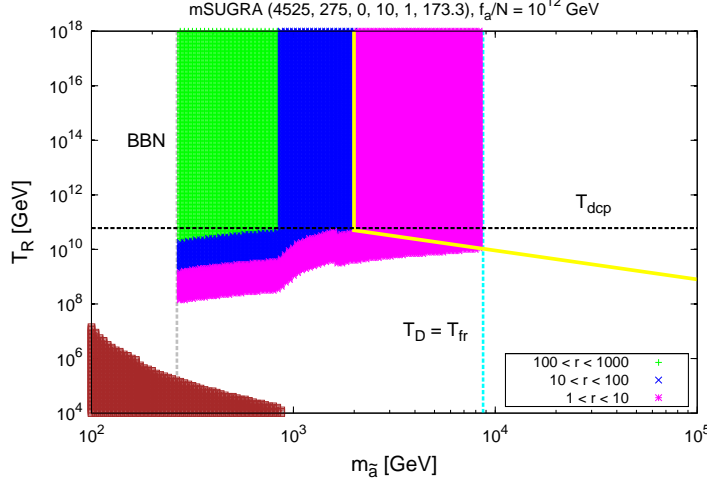


Figure 5: Plot of regions of $m_{\tilde{a}}$ vs. T_R plane where $T_{fr} < T_e$ (right of yellow contour) and where *no* additional neutralino annihilation occurs (brown), in the BM1 (HB/FP) benchmark model. We also show regions of entropy generation r .

where $n_{\tilde{Z}_1}(T_D)$ is the total neutralino number density due to thermal (freeze-out) and non-thermal (axino decays) production. We can rewrite the above condition as:

$$Y_{\tilde{Z}_1}|_{T=T_D} = \left(Y_{\tilde{Z}_1}^{\tilde{a}} + Y_{\tilde{Z}_1}^{fr}(T_D) \right) > \frac{(90/\pi^2 g_*(T_D))^{1/2}}{4\langle\sigma v\rangle M_P T_D}, \quad (7.7)$$

where for $r > 1$ we have $Y_{\tilde{Z}_1}^{\tilde{a}} = Y_{\tilde{a}}/r$ and $Y_{\tilde{Z}_1}^{fr}(T_D)$ is given by Eq. C.12. If this condition is satisfied, then additional neutralino annihilation will occur at $T \sim T_D$.

The relevant regions are shown in the T_R vs. $m_{\tilde{a}}$ plane for $f_a/N = 10^{12}$ GeV in Fig. 5 for BM1 and in Fig. 6 for BM2. The magenta, blue and green regions show ranges of different entropy dilution factors r , while the brown-shaded region is where there are not enough neutralinos produced through axino decays to cause re-annihilation. The region to the left of the BBN line is excluded, since $T_D < 2$ MeV, and thus we see that for nearly all of the allowed parameter space, neutralino re-annihilation effects need to be included in our calculations of the neutralino relic density. We also show the (vertical, dotted) line where $T_D = T_{fr}$. The region to the right of this line is where $T_D > T_{fr}$ and the axino decay products are expected to thermalize before neutralino freeze-out.

A simple expression for the diminution of neutralinos from re-annihilation has been worked out in Ref. [18] in the sudden-decay approximation. Recasting the Boltzmann equation 7.1 in terms of the yield variable

$$\frac{dY_{\tilde{Z}_1}}{dt} = -\langle\sigma v\rangle Y_{\tilde{Z}_1}^2 s \quad (7.8)$$

and integrating from time $t = t_D$ to t gives

$$Y_{\tilde{Z}_1}^{-1}(T) = Y_{\tilde{Z}_1}^{-1}(T_D) - \langle\sigma v\rangle \left(\frac{s}{H} - \frac{s(T_D)}{H(T_D)} \right) \simeq Y_{\tilde{Z}_1}^{-1}(T_D) + \frac{\langle\sigma v\rangle s(T_D)}{H(T_D)}. \quad (7.9)$$

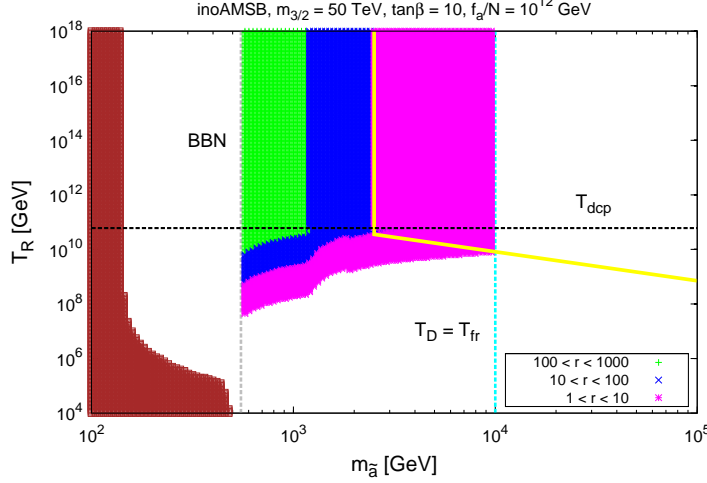


Figure 6: Plot of regions of $m_{\tilde{a}}$ vs. T_R plane where $T_{fr} < T_e$ (right of yellow contour) and where *no* additional neutralino annihilation occurs (brown), in the BM2 (inoAMSB) benchmark model. We also show regions of entropy generation r .

where $Y_{\tilde{Z}_1}(T_D) = Y_{\tilde{Z}_1}^{fr} + Y_{\tilde{Z}_1}^{\tilde{a}}$, and for $T_R \gtrsim 10^4$ GeV, the decay contribution can be huge, so that $Y_{\tilde{Z}_1}^{-1}(T_D)$ is small. Then Eq. 7.9 is dominated by the second term and

$$Y_{\tilde{Z}_1}(T) \simeq H(T_D)/\langle\sigma v\rangle s(T_D) \simeq Y_{\tilde{Z}_1}^{fr}(T_D) \quad (7.10)$$

Since the latter term is evaluated at $T = T_D$, it is much larger than $Y_{\tilde{Z}_1}^{fr}(T_{fr})$, and in fact the neutralino abundance turns out to be nearly the freeze-out abundance but evaluated at the much lower temperature T_D .

To exhibit the effect graphically, in Fig. 7 we plot the neutralino yield Y versus T_R for a). the BM1 benchmark and b). the BM2 benchmark. In both cases, we take $f_a/N = 10^{12}$ GeV and $m_{\tilde{a}} = 1$ TeV. The blue curve represents the sum of the thermal neutralino yield from freeze-out plus the neutralino yield from axino production and decay, where this term dominates for all but the lowest values of T_R in the plot. It increases with T_R as the thermal yield of axinos, Eq. 4.3, increases linearly with T_R . For T_R high enough that axinos can dominate the universe, the neutralino abundance is diluted by entropy production by the same factor as axinos are produced, and thus the curve becomes flat. The green curve is the second term of Eq. 7.9 and corresponds to the thermal neutralino yield, Eq. 7.4, but evaluated at T_D instead of T_{fr} . The red curve denotes the final neutralino yield, *i.e.* that given by Eq. 7.9. From Fig. 7 we see that, for $T_R \simeq 10^4$ GeV, the final neutralino yield ($Y_{\tilde{Z}_1}(T)$) is close to the naive sum of thermal and non-thermal production ($Y_{\tilde{Z}_1}(T_D)$) with a small suppression due to the re-annihilation effect. As T_R increases, $Y_{\tilde{Z}_1}^{\tilde{a}}$ increases and so does $Y_{\tilde{Z}_1}(T)$, but at a smaller rate, since the re-annihilation becomes more and more efficient. Once $T_R \simeq 10^5$ GeV, the annihilation term is efficient enough to re-annihilate all neutralinos down to their equilibrium value ($Y_{\tilde{Z}_1}^{fr}(T_D)$). Thus, for $T_R \gtrsim 10^5$ GeV, the neutralinos injected from axino decays can effectively thermalize to $Y_{\tilde{Z}_1}^{fr}(T_D)$ and the final

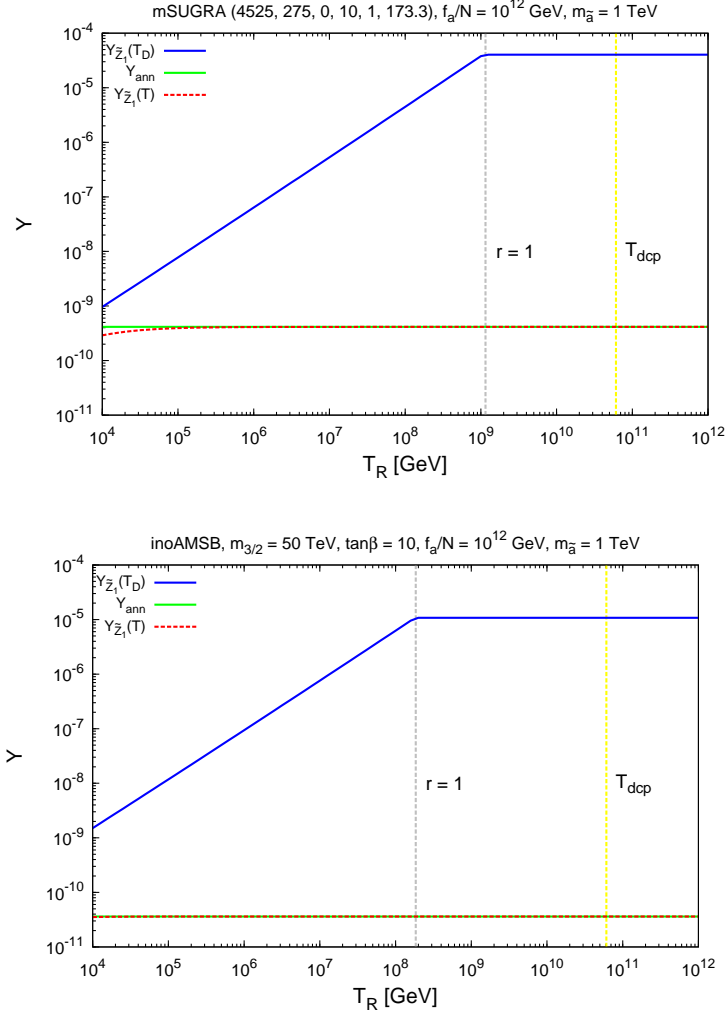


Figure 7: Plot of yield Y versus T_R for $f_a/N = 10^{12}$ GeV and $m_{\tilde{a}} = 1$ TeV for a) the FP model and b) the inoAMSB model.

neutralino yield becomes independent of the initial axino abundance. Since T_D is usually far below T_{fr} , Eq. 7.4 tells us that the neutralino yield $Y_{\tilde{Z}_1}(T) \simeq Y_{\tilde{Z}_1}^{fr}(T_D)$ will likely far exceed the thermal yield evaluated at T_{fr} , $Y_{\tilde{Z}_1}^{fr}(T_{fr})$.

For benchmarks BM1 and BM2, the region to the right of the yellow contour and to the left of the vertical blue line denotes where, in Figs. 5 and 6, we have $T_D < T_{fr} < T_e$. In this case, the thermal neutralino abundance must be calculated in a MD or DD universe. To illustrate, we show the various neutralino yields in Fig. 8 for benchmark BM1 with $m_{\tilde{a}} = 5$ TeV. The pink curve denotes the thermal neutralino abundance, which is constant versus T_R until $r > 1$, where the abundance becomes diluted by $1/r$ and begins to decrease. At $T_R \sim 2 \times 10^{10}$ GeV, T_e begins to exceed T_{fr} , the neutralino freeze-out happens in a MD universe, and suffers an increase. The corresponding freeze-out temperature is denoted by the azure colored curve, and the right-hand y -axis: we see that T_{fr} drops from ~ 3.8

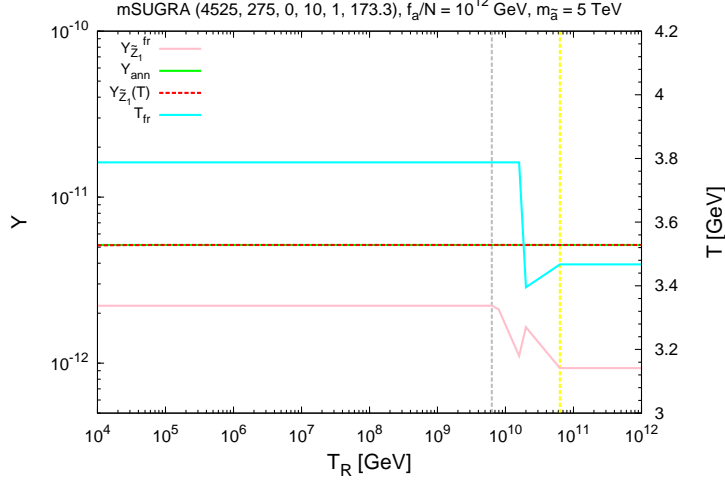


Figure 8: Plot of yield Y versus T_R for $f_a/N = 10^{12}$ GeV and $m_{\tilde{a}} = 5$ TeV for the BM1 (HB/FP) model. The dashed gray line shows where $r = 1$ and the yellow line shows where $T_R = T_{dcp}$.

GeV to ~ 3.5 GeV as we move from a RD to a MD universe. From Fig. 8 we see that the change in $Y_{\tilde{Z}_1}^{fr}$ is inconsequential to the final neutralino yield ($Y_{\tilde{Z}_1}(T)$), since this is determined by the re-annihilation term (green curve), and is insensitive to the thermal neutralino abundance, at least in this case.

8. Algorithm for DM abundance in $a\tilde{Z}_1$ DM scenario

In this section, we list our algorithm for evaluating the relic density of mixed $a\tilde{Z}_1$ CDM in the PQMSSM. We proceed as follows. First, extract an effective value of $\langle\sigma v\rangle$ by matching Eq. 7.4 onto the $\Omega_{\tilde{Z}_1} h^2$ result from the IsaReD subroutine of Isajet (the effective $\langle\sigma v\rangle$ value is shown in Table 1). Then:

- If $T_D < T_{BBN}$ (where T_{BBN} is taken as 2 MeV), regard as BBN excluded[35].
- If $T_D > T_{fr}$, then $\Omega_{\tilde{Z}_1} h^2 = \Omega_{\tilde{Z}_1}^{std} h^2$, given by the IsaReD output.
- If $T_D < T_{fr}$ and $T_D > T_{BBN}$, then
 - If $r > 1$: (Case of axino domination with $T_e > T_D$)
 - * If \tilde{Z}_1 re-annihilate (Eq. 7.7 satisfied), then calculate $Y_{\tilde{Z}_1}$ using Eq. 7.9 with $Y_{\tilde{Z}_1}(T_D) = Y_{\tilde{Z}_1}^{fr} + Y_{\tilde{Z}_1}^{\tilde{a}}$, where $Y_{\tilde{Z}_1}^{fr}$ is given by Eq. C.12 and $Y_{\tilde{Z}_1}^{\tilde{a}} = Y_{\tilde{a}}/r$.
 - * If \tilde{Z}_1 does not re-annihilate (Eq. 7.7 not satisfied), then $Y_{\tilde{Z}_1} = Y_{\tilde{Z}_1}^{fr} + Y_{\tilde{Z}_1}^{\tilde{a}}$, where $Y_{\tilde{Z}_1}^{fr}$ is given by Eq. C.12 and $Y_{\tilde{Z}_1}^{\tilde{a}} = Y_{\tilde{a}}/r$.
 - If $r < 1$: (axino non-domination)
 - * If neutralinos re-annihilate (Eq. 7.7 holds), then yield given by Eq. 7.9 with $Y_{\tilde{Z}_1}^{fr}$ given by Eq. 7.4 and $Y_{\tilde{Z}_1}^{\tilde{a}} = Y_{\tilde{a}}$.

* If neutralinos do not re-annihilate (Eq. 7.7 does not hold), then yield given by $Y_{\tilde{Z}_1}^{fr} + Y_{\tilde{Z}_1}^{\tilde{a}}$ with $Y_{\tilde{Z}_1}^{fr}$ given by Eq. 7.4 and $Y_{\tilde{Z}_1}^{\tilde{a}} = Y_{\tilde{a}}$.

- Now add in axion contribution to relic abundance Eq. B.14
- Final dark matter abundance is given by: $\Omega_{a\tilde{Z}_1} h^2 = \Omega_{\tilde{Z}_1} h^2 + \Omega_a h^2$.

9. Numerical results

In this section, we present results for the relic abundance of mixed $a\tilde{Z}_1$ CDM for benchmarks BM1 and BM2 in the PQMSSM. Our first results are shown in Fig. 9, where we plot the neutralino abundance, $\Omega_{\tilde{Z}_1} h^2$, the axion abundance, $\Omega_a h^2$, and their combination, $\Omega_{a\tilde{Z}_1} h^2$, versus $m_{\tilde{a}}$ for $f_a/N = 10^{12}$ GeV, with $T_R = 10^{10}$ GeV. We take the initial axion field value $\theta_i = 0.498$ for the BM1 benchmark case shown in frame a). and we take $\theta_i = 0.675$ for the BM2 benchmark in frame b). These values tune the total dark matter abundance to the WMAP value for the case where $T_D > T_{fr}$. From frame a)., we find the region to the left of the dashed gray line is excluded by BBN constraints on late decaying neutral particles, since $T_D < 2$ MeV. For $m_{\tilde{a}}$ values just beyond the BBN constraint, the naive expectation is that the neutralino abundance is determined by the thermal axino production rate, and indeed Fig. 2 suggests the abundance $\Omega_{\tilde{Z}_1} h^2 \sim 10^7$. Instead, the actual abundance is several orders of magnitude below this, but still far above the measured DM value. In this case, the large thermal axino production rate is followed by decays to neutralinos at $T = T_D$. As relic neutralinos fill the universe they proceed to annihilate, so that their final abundance is determined by Eq. 7.9. Since in this region $\Omega_{\tilde{Z}_1} h^2 \sim 1/T_D$, and since $T_D \sim m_{\tilde{a}}^{3/2}$, we find the neutralino abundance decreasing with increasing $m_{\tilde{a}}$. The kink in frame a). at $m_{\tilde{a}} \sim 900$ GeV occurs due to turn-on of the $\tilde{a} \rightarrow \tilde{g}g$ decay mode, which increases $\Gamma_{\tilde{a}}$, thus decreasing $\Omega_{\tilde{Z}_1} h^2$ even further. The jog at $m_{\tilde{a}} \sim 1.6$ TeV is caused by a change in the g_* value due to the addition of quark and gluon degrees of freedom after the QCD phase transition. While $\Omega_{\tilde{Z}_1} h^2$ is decreasing with increasing $m_{\tilde{a}}$, it reaches 0.11 at $m_{\tilde{a}} \sim 6$ TeV and continues dropping until T_D exceeds T_{fr} . At this point, the thermal \tilde{Z}_1 abundance assumes its traditional value of $\Omega_{\tilde{Z}_1}^{std} h^2 \sim 0.05$ since now axinos decay before freeze-out. For $m_{\tilde{a}} \gtrsim 8.5$ TeV, the CDM is a nearly equal mix of axions and neutralinos. While $T_D > 1$ GeV (for high $m_{\tilde{a}}$), the axion abundance assumes the form as given in Eq. 6.1. However, if considering lower values of $m_{\tilde{a}}$, then $r > 1$ and $T_D < 1$ GeV, so that the axion abundance is diluted by entropy production from axino decay. As $m_{\tilde{a}}$ increases, the axion dilution becomes lessened until T_D exceeds ~ 1 GeV, after which the axion abundance remains fixed.

In frame b)., for the inoAMSB model, we again see that the neutralino abundance is large at small $m_{\tilde{a}}$: $\Omega_{\tilde{Z}_1} h^2 \sim 10$ for $m_{\tilde{a}} \simeq 600$ GeV. It decreases steadily with $m_{\tilde{a}}$ due to the increasing T_D . The curve does reach a point where the neutralino abundance matches the WMAP7 measured value, at $m_{\tilde{a}} \sim 1.5$ TeV. In fact, the neutralino production via axino decay and subsequent re-annihilation effect offers an elegant means to enhance the WIMP relic density in SUSY models with higgsino or wino-like WIMPs. This mechanism offers an alternative[26] to the neutralino abundance enhancement via moduli decays as proposed

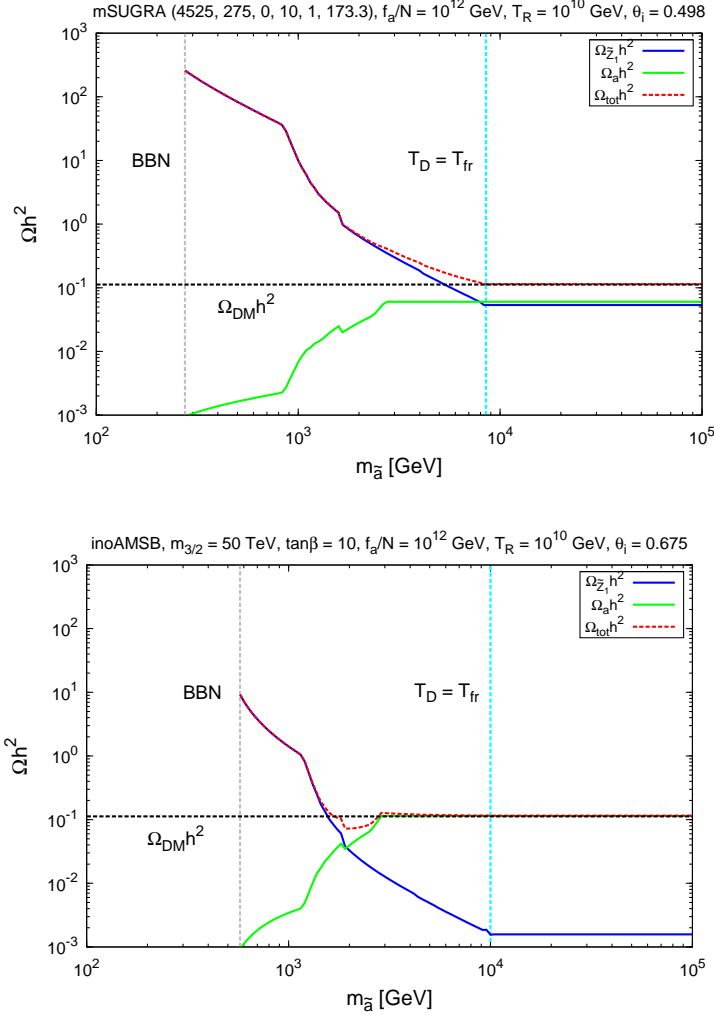


Figure 9: Plot of neutralino and axion relic densities Ωh^2 versus $m_{\tilde{a}}$ for $f_a/N = 10^{12}$ GeV and $T_R = 10^{10}$ GeV for a) the HB/FP model and b) the inoAMSB model.

by Morio and Randall[36] for AMSB, and as proposed by Kane et al. to explain the Pamela/Fermi cosmic ray anomalies[37]. By the time T_D exceeds T_{fr} , the axion abundance has assumed the value given by Eq. 6.1, and $\Omega_{\tilde{Z}_1} h^2 \sim 10^{-3}$, as given in Table 1.

In Fig. 10, we show the mixed $a\tilde{Z}_1$ abundance versus f_a/N for fixed $m_{\tilde{a}} = 1$ TeV and $T_R = 10^{10}$ GeV for a). BM1 and b). the BM2 benchmarks. In the HB/FP case of frame a)., we see that for low f_a/N , the axino width $\Gamma_{\tilde{a}}$ is large, and T_D exceeds T_{fr} , so that axinos decay before freeze-out and the neutralino relic density assumes its standard value of $\Omega_{\tilde{Z}_1}^{std} h^2 = 0.05$ in this case. Meanwhile, the axion density is extremely small due to the low value of f_a/N . As f_a/N increases, the axion abundance naturally increases, while the neutralino abundance remains constant until around $f_a/N \sim 10^{10}$ GeV, where T_D falls below T_{fr} . For higher f_a/N values, T_D continues to fall and since $\Omega_{\tilde{Z}_1} h^2 \sim T_D^{-1}$, the neutralino abundance steadily increases. At the point where $r = 1$ is

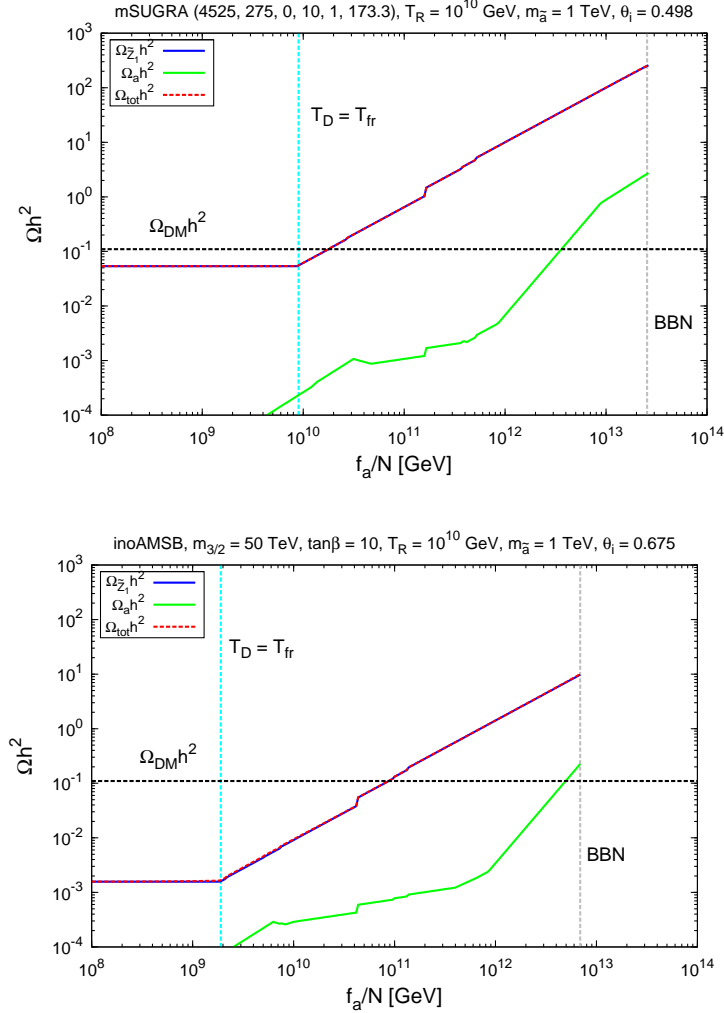


Figure 10: Plot of neutralino and axion relic densities Ωh^2 versus f_a/N for $m_{\tilde{a}} = 1$ TeV and $T_R = 10^{10}$ GeV for *a*) the HB/FP model and *b*) the inoAMSB model.

reached ($f_a/N \sim 2 \times 10^{10}$ GeV), entropy injection from axino decay causes a small decline in the otherwise steadily increasing axion abundance. The general behavior in frame *b*). for the inoAMSB model is similar to that of frame *a*). Nowhere in these two plots does the axion abundance exceed the neutralino abundance. This is merely a reflection of our choice of $m_{\tilde{a}} = 1$ TeV and θ_i ; for higher values of $m_{\tilde{a}}$, the value of T_D increases, resulting in a decrease of $\Omega_{\tilde{Z}_1} h^2$ when re-annihilation dominates the neutralino relic abundance.

In Fig. 11, we show the mixed dark matter relic abundance versus T_R for fixed $f_a/N = 10^{12}$ GeV and fixed $m_{\tilde{a}} = 1$ TeV, for benchmarks BM1 and BM2. In this case, T_D is fixed throughout the plots, and so $\Omega_{\tilde{Z}_1} h^2$ is nearly constant everywhere except at low $T_R \sim 10^4$ GeV, where thermal axino production is somewhat suppressed, and fewer neutralinos are produced at T_D to enter the re-annihilation process. Since f_a/N is fixed, the axion abundance is also constant throughout much of the plot. At $T_R \gtrsim 10^8 - 10^9$ GeV, we

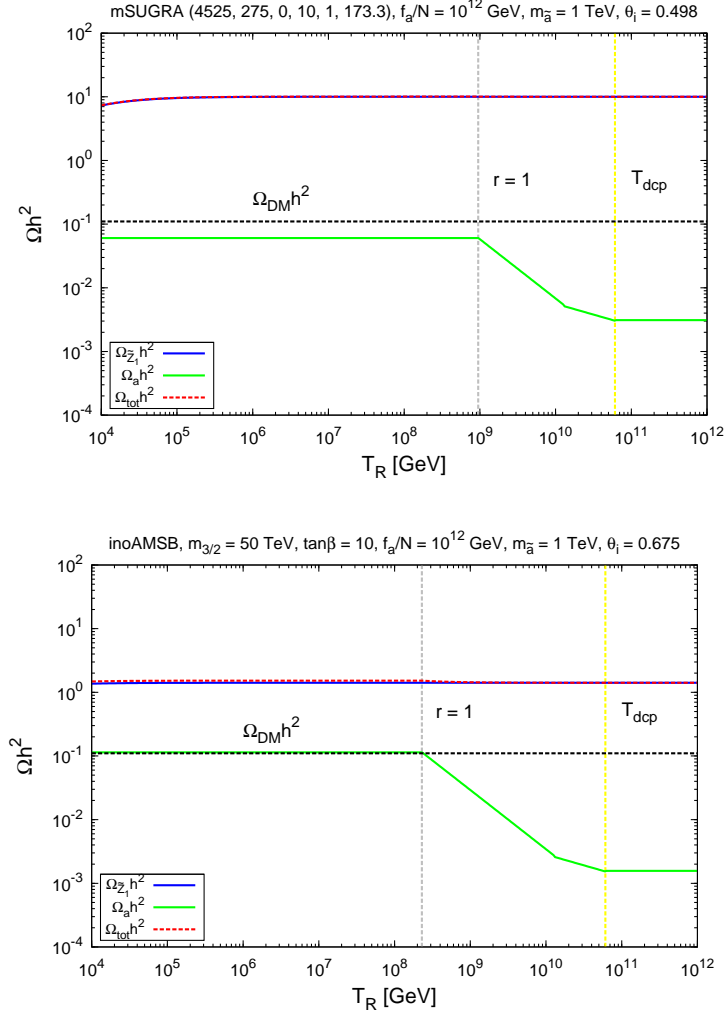


Figure 11: Plot of neutralino and axion relic densities Ωh^2 versus T_R for $m_{\tilde{a}} = 1$ TeV and $f_a/N = 10^{12}$ GeV for a) the HB/FP model and b) the inoAMSB model.

enter the region where axinos can dominate the universe ($r > 1$), and entropy production from axino decay diminishes the axion abundance. For even higher values of $T_R > T_{dcp}$, the axino production rate becomes independent of T_R , and the entropy injection ratio r becomes constant with T_R . While the neutralino abundance dominates the axion abundance in these frames, again, this is just a reflection of the value of $m_{\tilde{a}}$ chosen; for higher $m_{\tilde{a}}$, T_D will increase, leading to a diminution of $\Omega_{\tilde{Z}_1} h^2$.

We have seen that over most of parameter space with $T_D < T_{fr}$, $\Omega_{\tilde{Z}_1} h^2 \sim 1/T_D \sim \Gamma_{\tilde{a}}^{-1/2} \sim (f_a/N)/m_{\tilde{a}}^{3/2}$, with little dependence on T_R . Hence, a good way to display the relic density of dark matter in the mixed $a\tilde{Z}_1$ CDM scenario is to display it in the $m_{\tilde{a}}$ vs. (f_a/N) plane for benchmarks BM1 and BM2. This plane is shown in Fig. 12a). for BM1 and frame b). for BM2. Here, we take $\theta_i = 0.498$ so as to normalize the relic density $\Omega_{a\tilde{Z}_1} h^2$ to the measured value 0.1123 when $T_D > T_{fr}$ and $f_a/N = 10^{12}$ GeV. The black contour denotes

the line where $T_D = T_{fr}$: below and right of this contour, the neutralino relic density is given by its usual thermal abundance, which is $\Omega_{\tilde{Z}_1} h^2 = 0.05$ for the BM1 case in frame *a*). In this region, the axion abundance increases with increasing f_a/N , so that $\Omega_{a\tilde{Z}_1} h^2 = 0.1123$ at $f_a/N = 10^{12}$ GeV by design, with a roughly even admixture of mixed higgsino and axion dark matter in the narrow azure-shaded region. In the region to the left of the $T_D = T_{fr}$ contour, the neutralino abundance rapidly increases, and we have regions of dominantly WIMP CDM.

In frame *b*). for BM2, we again adjust θ_i so that the total relic density equals the measured value for $T_D > T_{fr}$ with $f_a/N = 10^{12}$ GeV. We see qualitatively similar behavior as in frame *a*). The azure region for $T_D > T_{fr}$ (right-side of plot) has $\Omega_{\tilde{Z}_1} \sim 0.02$, and so is axion-dominated, while the azure region for $T_D < T_{fr}$ is wino-dominated. In the region with $T_D < T_{fr}$, the relic abundance of winos rapidly increases as we move to smaller $m_{\tilde{a}}$ or larger f_a/N values.

From the above results for the benchmarks BM1 and BM2, we see that the $a\tilde{Z}_1$ scenario can be classified into two main cases:

- *A*): decoupled axino ($T_D > T_{fr}$)
- *B*): axino enhanced DM ($T_D < T_{fr}$) .

Case *A*) happens for high T_D values, which are obtained at low f_a and/or high $m_{\tilde{a}}$, as seen in Figs. 9 and 10. In this scenario, the axino has no effect on the DM relic density, which can be a mixture of axions and neutralinos. Since the axion mis-alignment angle (θ_i) can always be adjusted so that $\Omega_a h^2 = 0.1123$, there is no lower bound on $\Omega_{\tilde{Z}_1} h^2$. Nonetheless the neutralino relic density must still satisfy:

$$\Omega_{\tilde{Z}_1} h^2 = \Omega_{\tilde{Z}_1}^{std} h^2 \leq 0.1123 \quad (T_D > T_{fr}) \quad (9.1)$$

where $\Omega_{\tilde{Z}_1}^{std} h^2$ is the standard neutralino freeze-out relic density in the MSSM, since there is no axino dilution or contribution in this case. Therefore, in Case *A*, any MSSM model satisfying Eq. 9.1 is allowed. For models where $\Omega_{\tilde{Z}_1}^{std} h^2 < 0.1123$, the remaining of the DM is composed of axions.

For Case *B*), $T_D < T_{fr}$, which is obtained at high f_a and/or low $m_{\tilde{a}}$. As shown in Figs. 7 and 8, for most of the parameter space considered here, the neutralino relic density is dominated by the annihilation term in Eq. 7.9. In this case the relic density can be approximated by:

$$\Omega_{\tilde{Z}_1} h^2 \simeq \Omega_{\tilde{Z}_1}^{std} h^2 \times \frac{T_{fr}}{T_D}. \quad (9.2)$$

Assuming $T_{fr} \sim m_{\tilde{Z}_1}/20$ and using Eqs. 5.2 and 3.2, we obtain:

$$\Omega_{\tilde{Z}_1} h^2 \simeq 25 \times \Omega_{\tilde{Z}_1}^{std} h^2 \left(\frac{m_{\tilde{Z}_1}}{100 \text{ GeV}} \right) \left(\frac{f_a/N}{10^{12} \text{ GeV}} \right) \left(\frac{1 \text{ TeV}}{m_{\tilde{a}}} \right)^{3/2} \left(1 - \frac{m_g^2}{m_a^2} \right)^{-3/2} \quad (9.3)$$

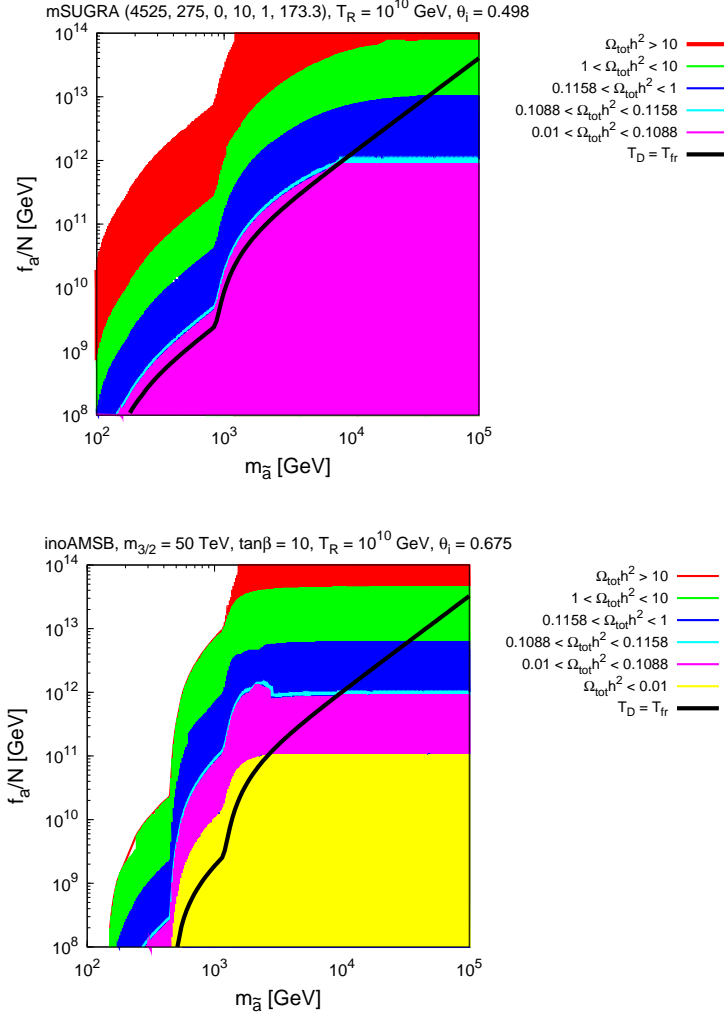


Figure 12: Regions of neutralino plus axion relic density $\Omega_{a\tilde{Z}_1} h^2$ in the $m_{\tilde{a}}$ vs. f_a/N plane for $T_R = 10^{10}$ GeV for a) the FP model and b) the inoAMSB model. The unshaded (white) regions are excluded by BBN bounds since $T_R < 2$ MeV.

where we assumed $m_{\tilde{a}} \gtrsim m_{\tilde{g}}$. Now imposing the DM relic density constraint (Eq. 9.1), we obtain:

$$\Omega_{\tilde{Z}_1}^{std} h^2 \lesssim 4 \times 10^{-3} \left(\frac{100 \text{ GeV}}{m_{\tilde{Z}_1}} \right) \left(\frac{10^{12} \text{ GeV}}{f_a/N} \right) \left(\frac{m_{\tilde{a}}}{1 \text{ TeV}} \right)^{3/2} \left(1 - \frac{m_{\tilde{g}}^2}{m_{\tilde{a}}^2} \right)^{3/2} (T_D < T_{fr}). \quad (9.4)$$

Therefore, in this case, the MSSM relic density has to be considerably suppressed in order to satisfy the above bound. Although the bound decreases with f_a and increases with $m_{\tilde{a}}$, for sufficiently low f_a and/or high $m_{\tilde{a}}$, then $T_D > T_{fr}$ and the bound in Eq. 9.1 must be used instead. In the case where $T_D < T_{fr}$, the DM will likely be composed mainly of relic neutralinos, unless $\Omega_{\tilde{Z}_1}^{std} h^2$ is much smaller than Eq. 9.4. We also point out that the approximate bound in Eq. 9.4 is a conservative one, since, for $m_{\tilde{a}} < m_{\tilde{g}}$, the bound would

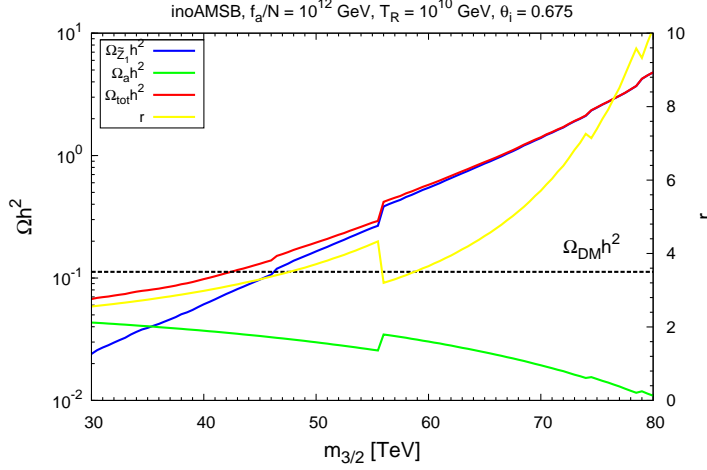


Figure 13: Neutralino, axion and total relic density for the inoAMSB model versus $m_{3/2}$ with $\tan\beta = 10$ and $\mu > 0$ and for $m_{\tilde{a}} = 2$ TeV and $\theta_i = 0.675$. We also show the value of r by the yellow curve, and the right-side axis.

be more strict.

To see how these conclusions depend on the SUSY spectrum, we show in Fig. 13 the neutralino, axion and summed relic abundance for the inoAMSB model versus $m_{3/2}$ for $\tan\beta = 10$ and $\mu > 0$. The results hardly change with varying $\tan\beta$ or μ . We also take $f_a/N = 10^{12}$ GeV, $m_{\tilde{a}} = 2$ TeV, $\theta_i = 0.675$ and $T_R = 10^{10}$ GeV. As $m_{3/2}$ increases, all the sparticle masses increase as well and so $\Gamma_{\tilde{a}}$ decreases. Once $m_{3/2} \simeq 50$ TeV, $m_{\tilde{g}} \simeq m_{\tilde{a}}/2$ and the bound in Eq. 9.4 can no longer be satisfied. The ratio of entropy injection r is shown as the yellow curve, against the right-hand y -axis. Since $r = 4m_{\tilde{a}}Y_{\tilde{a}}/3T_D$, and $T_D \sim \Gamma_{\tilde{a}}^{1/2}$, T_D decreases with increasing $m_{3/2}$, and the entropy ratio increases. This leads to a dilution of the axion relic density as shown in the plot. The jog in the curves around $m_{3/2} \sim 55$ TeV occurs due to a change in the degrees of freedom g_* .

10. Effect of saxion production and decay on relic abundance

We have seen so far that the relic neutralino abundance may be enhanced beyond usual expectations in the mixed $a\tilde{Z}_1$ scenario if $T_D < T_{fr}$. However, we have so far neglected a mandatory element of the axion supermultiplet: the spin-0, R -parity even saxion field s [38]. Saxions may be produced thermally in the early universe, either in thermal equilibrium for $T_R > T_{dcp}$ or via radiation and decay for $T_R < T_{dcp}$. Saxions can also be produced via coherent oscillations.

In an analagous manner to the axino case, the saxion field can dominate the energy density of the universe at early times, if its decay temperature (T_{D_s}) is smaller than the temperature (T_{e_s}) at which its energy density overcomes the radiation and axino energy densities. The saxion can decay into gluons and gluinos (and perhaps axions), depending on its mass and its (model dependent) couplings. As in the axino case, the saxion decay

will inject entropy at $T = T_{D_s}$, diluting the axino (if $T_D < T_{D_s}$), neutralino (if $T_{fr} > T_{D_s}$) and axion (if $T_a > T_{D_s}$) relic densities. Furthermore, if the $s \rightarrow \tilde{g}\tilde{g}$ branching ratio is considerable, saxion decays will also inject neutralinos through gluino cascade decays. In the case where a high rate of neutralino injection occurs after freeze-out, one must again consider a second possibility of neutralino re-annihilation which may enhance the neutralino abundance.

Since the saxion lifetime is comparable to the axino lifetime, it is possible that both saxions and axinos may co-dominate the universe. This makes a simplistic analysis of neutralino abundance difficult using the approach of this paper. To make matters worse, gravitinos may be produced thermally at significant rates for high enough T_R , and enjoy decays at time scales comparable to heavy axinos and saxions. Thus, gravitino production and decay may also enhance or diminish the neutralino abundance.

The proper treatment of such intricately coupled effects is best made by numerical solution of the coupled Boltzmann equations. This type of treatment has been initiated in Ref. [39], and will be reported at a future date.

11. Conclusions

In this paper, we have presented results of calculations of the dark matter abundance in supersymmetric models wherein the strong CP problem is solved by the Peccei-Quinn mechanism, and in which the neutralino is the LSP, so that dark matter consists of an axion/neutralino admixture. Since the $a\tilde{Z}_1$ CDM scenario boosts the dark matter abundance beyond the usual thermal neutralino production rates, we have presented results for two models that typically yield an underabundance of thermal neutralino dark matter: the HB/FP region of mSUGRA with a mixed higgsino-like neutralino and AMSB-type models with a wino-like neutralino. Our final results depend mainly on the temperature T_D at which heavy axinos finish their cascade decays to neutralinos.

In the case where $T_D > T_{fr}$, the neutralino abundance is given by its usual thermal abundance. In the case where there is an underabundance of neutralinos compared to the measured dark matter abundance, then the remainder can be comprised of axions. In the case of our two benchmark models, in the HB/FP region, we would obtain a nearly equal mixture of axions and mixed higgsino-like neutralinos, while in the BM2 case of the inoAMSB model, we would obtain a case with mainly axion CDM, along with a small admixture of wino-like neutralinos. The case of BM1 provides an instance where both WIMP and axion signals[43] could ultimately be found at dark matter detectors. In the case of BM2, only an axion signal might be discovered. The direct detection rates for wino-like WIMPs has been presented in Ref. [26]. These projected rates would have to be scaled down by a factor of ~ 70 since in this case wino-like WIMPs would only comprise $\sim 1/70$ of the total dark matter abundance.

In the case where $T_D < T_{fr}$, heavy axino decays in the early universe will inject additional neutralinos and entropy into the cosmic soup after neutralino freeze-out. The main effect here is that neutralino re-annihilation takes place at $T = T_D$, and one obtains a neutralino abundance as if the freeze-out temperature were replaced by T_D . In this case,

$\Omega_{\tilde{Z}_1} h^2 \sim 1/T_D$ instead of $1/T_{fr}$, and since $T_D < T_{fr}$, one obtains a greatly enhanced abundance of neutralinos beyond the usual expectation. The neutralino “production by decay and re-annihilation” mechanism can thus lead to enhanced production of wino-like or higgsino-like neutralinos– which naively give rise to an underabundance of dark matter– so that \tilde{Z}_1 s might comprise nearly all the abundance of dark matter. Also in this case, if $T_e > T_D$, then significant entropy production by decaying axinos can diminish the axion abundance. In this case, one might expect mainly wino-like or higgsino-like dark matter, with a small admixture of axions. Thus, the enhanced neutralino production via axino decay mechanism offers an alternative means to allow wino- or higgsino-like neutralinos to comprise the bulk of dark matter. In many respects, this mechanism may be preferred over the possibility of multi-TeV scale moduli field decay[36, 37], since it also allows for a solution to the strong CP problem.

Acknowledgments

This research was supported in part by the U.S. Department of Energy, by the Fulbright Program and CAPES (Brazilian Federal Agency for Post-Graduate Education).

A. Expansion rate of early universe

Here we briefly review the cosmology of an early axino dominated universe and in the next Section present the expressions for the axion relic density and neutralino yield used in Secs. 7-9.

First, we define several temperatures:

- T_e : temperature when the universe becomes axino (matter) dominated,
- T_S : temperature at which entropy injection due to axino decay starts,
- T_D : temperature at which entropy injection due to axino decay ends.

A.1 Matter dominated phase: $T_S < T < T_e$

In this phase, the universe is axino dominated, for which:

$$\rho_{\tilde{a}} = \rho_0 \frac{R_e^3}{R^3} \exp(-(t - t_e)\Gamma_{\tilde{a}}) \approx \rho_0 \frac{R_e^3}{R^3} \quad (\text{A.1})$$

$$H(T) = \sqrt{\frac{\rho_{\tilde{a}}}{3M_P^2}} \simeq \sqrt{\frac{\rho_0}{3M_P^2}} \left(\frac{R_e}{R} \right)^{3/2} \quad (\text{A.2})$$

where $R_e = R(T_e)$ and $\Gamma_{\tilde{a}}$, $\rho_{\tilde{a}}$, $Y_{\tilde{a}}$ and $m_{\tilde{a}}$ are the axino width, energy density, yield and mass, respectively. Here, $M_P = M_{Pl}/\sqrt{8\pi}$ (*i.e.* M_P is the reduced Planck mass), and we will use $g_{*S} = g_*$ since the temperatures we consider are all above $T_{BBN} \simeq 2$ MeV. By definition we have:

$$\rho_0 = \frac{\pi^2}{30} g_*(T_e) T_e^4 \quad \text{and} \quad T_e = \frac{4}{3} Y_{\tilde{a}} m_{\tilde{a}}. \quad (\text{A.3})$$

Since entropy is still conserved in this phase,

$$\frac{g_*(T)T^3}{g_*(T_e)T_e^3} = \left(\frac{R_e}{R}\right)^3, \quad (\text{A.4})$$

and hence

$$H(T) = \sqrt{\frac{\pi^2}{90}g_*(T)T_e} \frac{T^{3/2}}{M_P}. \quad (\text{A.5})$$

A.2 Decaying particle dominated phase: $T_D < T < T_S$

In this phase, the universe is dominated by a decaying particle[40], which gives:

$$\rho_{\tilde{a}} = \rho_0 \frac{R_e^3}{R^3} \exp(-(t - t_e)\Gamma_{\tilde{a}}) \approx \rho_0 \frac{R_e^3}{R^3} \quad (\text{A.6})$$

$$H(T) = \sqrt{\frac{\rho_{\tilde{a}}}{3M_P^2}} \approx \sqrt{\frac{\rho_0}{3M_P^2}} \left(\frac{R_e}{R}\right)^{3/2}. \quad (\text{A.7})$$

Entropy is no longer conserved, so that[32, 41]:

$$\frac{g_*(T)^2 T^8}{g_*(T_0)^2 T_0^8} = \left(\frac{R_0}{R}\right)^3. \quad (\text{A.8})$$

Using this relation, we obtain:

$$H(T) = H(T_D) \left(\frac{R(T_D)}{R(T)}\right)^{3/2} = H(T_D) \frac{g_*(T)T^4}{g_*(T_D)T_D^4}. \quad (\text{A.9})$$

But, at $T = T_D$ all the matter energy has been converted to radiation, hence

$$H(T_D) = \sqrt{\frac{\pi^2}{90}g_*(T_D)} \frac{T_D^2}{M_P} \quad \text{or} \quad (\text{A.10})$$

$$H(T) = \sqrt{\frac{\pi^2}{90}} \frac{g_*(T)}{\sqrt{g_*(T_D)}} \frac{T^4}{T_D^2 M_P} \quad (\text{A.11})$$

The decay temperature (T_D) and $\Gamma_{\tilde{a}}$ are related by $H(T_D) = \Gamma_{\tilde{a}}$, so that

$$\Gamma_{\tilde{a}}^2 = \frac{\pi^2}{90} g_*(T_D) \frac{T_D^4}{M_P^2}. \quad (\text{A.12})$$

A.3 Radiation dominated phase: $T < T_D$

In this phase the universe is radiation dominated, giving the standard expressions:

$$H(T) = \sqrt{\frac{\rho_\gamma}{3M_P^2}} = \sqrt{\frac{\pi^2}{90}g_*(T)} \frac{T^2}{M_P} \quad (\text{A.13})$$

and entropy is once again conserved:

$$\frac{g_*(T)T^3}{g_*(T_0)T_0^3} = \left(\frac{R_0}{R}\right)^3. \quad (\text{A.14})$$

B. Axion oscillation

The axion field starts to oscillate when²

$$3H(T_a) = m_a(T_a) \quad (\text{B.1})$$

where the temperature-dependent axion mass is given by

$$m_a(T) = \begin{cases} m_a, & \text{if } T < \Lambda \\ m_a b \left(\frac{\Lambda}{T}\right)^4, & \text{if } T > \Lambda \end{cases} \quad (\text{B.2})$$

with $b = 0.018$, $\Lambda = 0.2$ GeV and $m_a = 6.2 \times 10^{-3}/f_a$. Due to its temperature dependent mass, after oscillation begins, the axion energy density obeys

$$\frac{\rho_a(T)R(T)^3}{m_a(T)} = \text{constant}. \quad (\text{B.3})$$

If $T_a < T_D$, then the axion field starts to oscillate after the axino has decayed. In this case, the axion relic density is given by the standard expression[34, 42]:

$$\Omega_a^{\text{std}} h^2 = \begin{cases} 9.23 \times 10^{-3} \theta_i^2 f(\theta_i) \frac{1}{g_*(T_a)^{1/4}} \left(\frac{f_a}{10^{12}}\right)^{3/2}, & \text{if } f_a > \hat{f}_a \\ 1.32 \theta_i^2 f(\theta_i) \frac{1}{g_*(T_a)^{5/12}} \left(\frac{f_a}{10^{12}}\right)^{7/6}, & \text{if } f_a < \hat{f}_a \end{cases} \quad (\text{B.4})$$

where $\hat{f}_a = 9.9 \times 10^{16}$ GeV, $f(\theta_i) = \ln\left(\frac{e}{1-\theta_i^2/\pi^2}\right)^{7/6}$ and the standard oscillation temperature is given by

$$T_a^{\text{std}} = \begin{cases} 1.23 \times 10^2 \frac{1}{g_*(T_a)^{1/4}} \left(\frac{10^{12}}{f_a}\right)^{1/2}, & \text{if } f_a > \hat{f}_a \\ 8.71 \times 10^{-1} \frac{1}{g_*(T_a)^{1/12}} \left(\frac{10^{12}}{f_a}\right)^{1/6}, & \text{if } f_a < \hat{f}_a \end{cases} \quad (\text{B.5})$$

If instead $T_e < T_a$, then the axion density is diluted by the entropy ratio r so that

$$\Omega_a h^2 = \frac{1}{r} \times \Omega_a^{\text{std}} h^2 \quad (\text{B.6})$$

If $T_D < T_a < T_e$, the axion can start to oscillate in the matter dominated phase (MD) or the decaying dominate phase (DD). The relic densities for each case are:

- Matter dominated ($T_S < T_a < T_e$):

$$\Omega_a^{\text{MD}} h^2 = \begin{cases} 7.5 \times 10^{-5} \theta_i^2 f(\theta_i) T_D \left(\frac{f_a}{10^{12}}\right)^2, & \text{if } f_a > \hat{f}_a^{\text{MD}} \\ 1.4 \theta_i^2 f(\theta_i) \frac{1}{g_*(T_a)^{4/11}} \left(\frac{f_a}{10^{12}}\right)^{14/11} \frac{T_D}{T_e^{4/11}}, & \text{if } f_a < \hat{f}_a^{\text{MD}} \end{cases} \quad (\text{B.7})$$

with

$$\hat{f}_a^{\text{MD}} = 7.6 \times 10^{17} \frac{1}{\sqrt{g_*(T_a) T_e}} \quad (\text{B.8})$$

and T_a given by

²Here, we follow much of the notation given by Visinelli and Gondolo[42].

$$T_a^{MD} = \begin{cases} 6.1 \times 10^2 \left(\frac{1}{\sqrt{g_*(T_a)T_e}} \frac{10^{12}}{f_a} \right)^{2/3}, & \text{if } f_a > \hat{f}_a^{MD} \\ 8.6 \times 10^{-1} \left(\frac{1}{\sqrt{g_*(T_a)T_e}} \frac{10^{12}}{f_a} \right)^{2/11}, & \text{if } f_a < \hat{f}_a^{MD} \end{cases}. \quad (\text{B.9})$$

- Decaying particle dominated ($T_D < T_a < T_S$)[42]:

$$\Omega_a^{DD} h^2 = \begin{cases} 7.5 \times 10^{-5} \theta_i^2 f(\theta_i) T_D \left(\frac{f_a}{10^{12}} \right)^2, & \text{if } f_a > \hat{f}_a^{DD} \\ 1.72 \theta_i^2 f(\theta_i) \frac{g_*(T_D)^{1/4}}{\sqrt{g_*(T_a)}} T_D^2 \left(\frac{f_a}{10^{12}} \right)^{3/2}, & \text{if } f_a < \hat{f}_a^{DD} \end{cases} \quad (\text{B.10})$$

with

$$\hat{f}_a^{DD} = 5.69 \times 10^{20} \frac{\sqrt{g_*(T_D)}}{g_*(T_a)} T_D^2 \quad (\text{B.11})$$

and T_a given by:

$$T_a^{DD} = \begin{cases} 0.11 \times 10^2 \left(\frac{\sqrt{g_*(T_D)}}{g_*(T_a)} \frac{10^{12}}{f_a} T_D^2 \right)^{1/4}, & \text{if } f_a > \hat{f}_a^{DD} \\ 9.0 \times 10^{-1} \left(\frac{\sqrt{g_*(T_D)}}{g_*(T_a)} \frac{10^{12}}{f_a} T_D^2 \right)^{1/8}, & \text{if } f_a < \hat{f}_a^{DD} \end{cases}. \quad (\text{B.12})$$

Matching both solutions we have:

$$\begin{aligned} \left(\frac{f_a}{10^{12}} \right)^{5/22} &< 0.8 \frac{g_*(\bar{T}_a)^{3/22}}{g_*(T_D)^{1/4}} \frac{1}{T_D T_e^{4/11}} \rightarrow \text{MD case} \\ \left(\frac{f_a}{10^{12}} \right)^{5/22} &> 0.8 \frac{g_*(\bar{T}_a)^{3/22}}{g_*(T_D)^{1/4}} \frac{1}{T_D T_e^{4/11}} \rightarrow \text{DD case} \end{aligned}$$

or in terms of T_a :

$$\begin{aligned} T_a &> T_S \rightarrow \text{MD case} \\ T_a &< T_S \rightarrow \text{DD case} \end{aligned}$$

where

$$T_S = \left(\frac{g_*(T_D)}{g_*(T_a^{(A)})} T_e T_D^4 \right)^{1/5} \quad (\text{B.13})$$

To summarize:

$$\Omega_a h^2 = \begin{cases} \Omega_a^{std} h^2 / r, & \text{if } T_e < T_a \\ \Omega_a^{MD} h^2, & \text{if } T_S < T_a < T_e \\ \Omega_a^{DD} h^2, & \text{if } T_D < T_a < T_S \\ \Omega_a^{std} h^2, & \text{if } T_a < T_D \end{cases}, \quad (\text{B.14})$$

where r is the entropy injection ratio as usual.

C. Neutralino yield

The neutralino will decouple from the thermal bath when

$$\langle\sigma v\rangle n_{\tilde{Z}_1}(T_{fr}) = H(T_{fr}) \quad (\text{C.1})$$

where

$$n_{\tilde{Z}_1}(T) = 2 \left(\frac{mT}{2\pi} \right)^{3/2} e^{-m/T}. \quad (\text{C.2})$$

In a radiation dominated universe, the neutralino yield is given by:

$$Y_{\tilde{Z}_1}(T_{fr}) = \frac{H(T_{fr})}{\langle\sigma v\rangle s(T_{fr})}, \quad (\text{C.3})$$

while in a matter dominated universe:

$$Y_{\tilde{Z}_1}(T_{fr}) = \frac{3}{2} \frac{H(T_{fr})}{\langle\sigma v\rangle s(T_{fr})}. \quad (\text{C.4})$$

As in the axion case, the neutralino can freeze-out before the universe becomes matter dominated ($T_{fr} > T_e$), during the MD phase ($T_S < T_{fr} < T_e$), during the DD phase ($T_D < T_{fr} < T_S$) or during the radiation dominated phase ($T_{fr} < T_D$). The neutralino yields for each of these scenarios are listed below.

- Standard case ($T_{fr} < T_D$):

$$Y_{\tilde{Z}_1}^{std}(T_{fr}) = \frac{(90/\pi^2 g_*(T_{fr}))^{1/2}}{4\langle\sigma v\rangle M_P T_{fr}} \quad (\text{C.5})$$

where the freeze-out temperature is given by

$$T_{fr}^{std} = m_{\tilde{Z}_1} / \ln \left[\frac{3\sqrt{5}\langle\sigma v\rangle M_P m_{\tilde{Z}_1}^{3/2}}{\pi^{5/2} T_{fr}^{1/2} g_*^{1/2}(T_{fr})} \right]. \quad (\text{C.6})$$

- MD case ($T_S < T_{fr} < T_e$):

$$Y_{\tilde{Z}_1}^{MD}(T_D) = \frac{3}{2} Y_{\tilde{Z}_1}^{std}(T_{fr}^{MD}) \frac{T_D}{\sqrt{T_e T_{fr}^{MD}}} \quad (\text{C.7})$$

where the freeze-out temperature T_{fr}^{MD} is given by:

$$T_{fr}^{MD} = m_{\tilde{Z}_1} / \ln \left[\frac{3\sqrt{5}\langle\sigma v\rangle M_P m_{\tilde{Z}_1}^{3/2}}{\pi^{5/2} g_*^{1/2}(T_{fr}^{MD}) T_e^{1/2}} \right]. \quad (\text{C.8})$$

- DD case ($T_D < T_{fr} < T_S$):

$$Y_{\tilde{Z}_1}^{DD}(T_D) = \frac{3}{2} Y_{\tilde{Z}_1}^{std}(T_{fr}^{DD}) \frac{g_*^{1/2}(T_D)}{g_*^{1/2}(T_{fr}^{DD})} \left(\frac{T_D}{T_{fr}^{DD}} \right)^3 \quad (C.9)$$

where the freeze-out temperature is given by

$$T_{fr}^{DD} = m_{\tilde{Z}_1} / \ln \left[\frac{3\sqrt{5} \langle \sigma v \rangle M_P m_{\tilde{Z}_1}^{3/2} g_*^{1/2}(T_D) T_D^2}{\pi^{5/2} g_*(T_{fr}^{DD}) (T_{fr}^{DD})^{5/2}} \right]. \quad (C.10)$$

- Case when $T_{fr} > T_e$:

$$Y_{\tilde{Z}_1}(T_D) = Y_{\tilde{Z}_1}^{std}(T_{fr}^{std})/r = Y_{\tilde{Z}_1}^{std}(T_{fr}^{std}) \times \frac{T_e}{T_D}. \quad (C.11)$$

To summarize:

$$Y_{\tilde{Z}_1}(T_D) = \begin{cases} Y_{\tilde{Z}_1}^{std}(T_{fr}^{std})/r, & \text{if } T_e < T_{fr} \\ Y_{\tilde{Z}_1}^{MD}, & \text{if } T_S < T_{fr} < T_e \\ Y_{\tilde{Z}_1}^{DD}, & \text{if } T_D < T_{fr} < T_S \\ Y_{\tilde{Z}_1}^{std}(T_{fr}^{std}), & \text{if } T_{fr} < T_D \end{cases} \quad (C.12)$$

where

$$T_S = \left(\frac{g_*(T_D)}{g_*(T_{fr}^{(A)})} T_D^4 T_e \right)^{1/5}. \quad (C.13)$$

References

- [1] H. Baer and X. Tata, *Weak Scale Supersymmetry: From Superfields to Scattering Events*, (Cambridge University Press, 2006).
- [2] H. Baer, V. Barger, A. Lessa and X. Tata, *J. High Energy Phys.* **1006** (2010) 102.
- [3] G. 't Hooft, *Phys. Rev. Lett.* **37** (1976) 8.
- [4] For a recent review, see P. Sikivie, [hep-ph/0509198](#); M. Turner, *Phys. Rept.* **197** (1990) 67; J. E. Kim and G. Carosi, *Rev. Mod. Phys.* **82** (2010) 557.
- [5] For a review, see J. E. Kim, *Phys. Rept.* **150** (1987) 1.
- [6] For a comprehensive discussion, see M. Pospelov and A. Ritz, *Annals Phys.* **318** (2005) 119.
- [7] R. Peccei and H. Quinn, *Phys. Rev. Lett.* **38** (1977) 1440 and *Phys. Rev.* **D 16** (1977) 1791.
- [8] S. Weinberg, *Phys. Rev. Lett.* **40** (1978) 223; F. Wilczek, *Phys. Rev. Lett.* **40** (1978) 279.
- [9] J. E. Kim, *Phys. Rev. Lett.* **43** (1979) 103; M. A. Shifman, A. Vainshtein and V. I. Zakharov, *Nucl. Phys.* **B 166** (1980) 493.
- [10] M. Dine, W. Fischler and M. Srednicki, *Phys. Lett.* **B 104** (1981) 199; A. P. Zhitnitskii, *Sov. J. Nucl.* **31** (1980) 260.
- [11] D. Dicus, E. Kolb, V. Teplitz and R. Wagoner, *Phys. Rev.* **D 18** (1978) 1829 and *Phys. Rev.* **D 22** (1980) 839; for a review, see G. Raffeldt, [hep-ph/0611350](#).
- [12] H. P. Nilles and S. Raby, *Nucl. Phys.* **B 198** (1982) 102; J. E. Kim and H. P. Nilles, *Phys. Lett.* **B 138** (1984) 150. J. E. Kim, *Phys. Lett.* **B 136** (1984) 378.

- [13] P. Svrcek and E. Witten, *J. High Energy Phys.* **0606** (2006) 051.
- [14] K. Rajagopal, M. Turner and F. Wilczek, *Nucl. Phys.* **B 358** (1991) 447.
- [15] L. Covi, J. E. Kim and L. Roszkowski, *Phys. Rev. Lett.* **82** (1999) 4180; L. Covi, H. B. Kim, J. E. Kim and L. Roszkowski, *J. High Energy Phys.* **0105** (2001) 033.
- [16] For recent reviews of axino dark matter, see F. Steffen, *Eur. Phys. J.* **C 59** (2009) 557; L. Covi and J. E. Kim, *New J. Phys.* **11** (2009) 105003.
- [17] H. Baer, A. Box and H. Summy, *J. High Energy Phys.* **0908** (2009) 080.
- [18] K-Y. Choi, J. E. Kim, H. M. Lee and O. Seto, *Phys. Rev.* **D 77** (2008) 123501.
- [19] E. Komatsu *et al.* (WMAP collaboration), arXiv:1001.4538 (2010).
- [20] For a recent review, see R. Arnowitt and P. Nath, arXiv:0912.2273 (2009)
- [21] K. L. Chan, U. Chattopadhyay and P. Nath, *Phys. Rev.* **D 58** (1998) 096004; J. Feng, K. Matchev and T. Moroi, *Phys. Rev. Lett.* **84** (2000) 2322 and *Phys. Rev.* **D 61** (2000) 075005; see also H. Baer, C. H. Chen, F. Paige and X. Tata, *Phys. Rev.* **D 52** (1995) 2746 and *Phys. Rev.* **D 53** (1996) 6241; H. Baer, C. H. Chen, M. Drees, F. Paige and X. Tata, *Phys. Rev.* **D 59** (1999) 055014; for a model-independent approach, see H. Baer, T. Krupovnickas, S. Profumo and P. Ullio, *J. High Energy Phys.* **0510** (2005) 020.
- [22] L. Randall and R. Sundrum, *Nucl. Phys.* **B 557** (1999) 79; G. Giudice, M. Luty, H. Murayama and R. Rattazzi, *J. High Energy Phys.* **9812** (1998) 027.
- [23] S. P. de Alwis, *J. High Energy Phys.* **1003** (2010) 078.
- [24] H. Baer, S. P. de Alwis, K. Givens, S. Rajagopalan and H. Summy, *J. High Energy Phys.* **1005** (2010) 069; H. Baer, S. P. de Alwis, K. Givens, S. Rajagopalan and W. Sreethawong, *J. High Energy Phys.* **1101** (2011) 005.
- [25] H. Baer and A. Box, *Eur. Phys. J.* **C 68** (2010) 523; H. Baer, A. Box and H. Summy, *J. High Energy Phys.* **1010** (2010) 023.
- [26] H. Baer, R. Dermisek, S. Rajagopalan and H. Summy, *JCAP***1007** (2010) 014.
- [27] ISAJET, by H. Baer, F. Paige, S. Protopopescu and X. Tata, [hep-ph/0312045](#); see also H. Baer, J. Ferrandis, S. Kraml and W. Porod, *Phys. Rev.* **D 73** (2006) 015010.
- [28] F. Paige, S. Protopopescu, H. Baer and X. Tata, [hep-ph/0312045](#);
<http://www.nhn.ou.edu/~isajet/>
- [29] H. Baer, C. Balazs and A. Belyaev, *J. High Energy Phys.* **0203** (2002) 042.
- [30] A. Brandenburg and F. Steffen, *JCAP***0408** (2004) 008.
- [31] A. Strumia, *J. High Energy Phys.* **1006** (2010) 036.
- [32] R. J. Scherrer and M. S. Turner, *Phys. Rev.* **D 31** (1985) 681.
- [33] L. F. Abbott and P. Sikivie, *Phys. Lett.* **B 120** (1983) 133; J. Preskill, M. Wise and F. Wilczek, *Phys. Lett.* **B 120** (1983) 127; M. Dine and W. Fischler, *Phys. Lett.* **B 120** (1983) 137; M. Turner, *Phys. Rev.* **D 33** (1986) 889.
- [34] L. Visinelli and P. Gondolo, *Phys. Rev.* **D 80** (2009) 035024.
- [35] K. Jedamzik, *Phys. Rev.* **D 70** (2004) 063524 and *Phys. Rev.* **D 74** (2006) 103509.

- [36] T. Moroi and L. Randall, *Nucl. Phys.* **B 570** (2000) 455; B. Acharya, G. Kane, S. Watson and P. Kumar, *Phys. Rev.* **D 80** (2009) 083529.
- [37] P. Grajek, G. Kane, D. Phalen, A. Pierce and S. Watson, *Phys. Rev.* **D 79** (2009) 043506; G. Kane, R. Lu and S. Watson, *Phys. Lett.* **B 681** (2009) 151. D. Feldman, G. Kane, R. Lu and B. Nelson, *Phys. Lett.* **B 687** (2010) 363.
- [38] J. E. Kim, *Phys. Lett.* **B 67** (1991) 3465; D. H. Lyth, *Phys. Rev.* **D 48** (1993) 4523; S. Chang and H. B. Kim, *Phys. Rev. Lett.* **77** (1996) 591; M. Hashimoto, K. Izawa, M. Yamaguchi and T. Yanagida, *Phys. Lett.* **B 437** (1998) 44; T. Asaka and M. Yamaguchi, *Phys. Rev.* **D 59** (1999) 125003; J. Hasenkamp and J. Kersten, *Phys. Rev.* **D 82** (2010) 115029; H. Baer, S. Kraml, A. Lessa and S. Sekmen, arXiv:1012.3769.
- [39] H. Baer, A. Lessa, S. Rajagopalan and W. Sreethawong, to appear.
- [40] J. McDonald, *Phys. Rev.* **D 43** (1991) 1063; C. Pallis, *Astropart. Phys.* **21** (2004) 689.
- [41] G. Lazarides, C. Panagiotakapoulos and Q. Shafi, *Phys. Lett.* **B 192** (1987) 323; G. Lazarides, R. Schaefer, D. Seckel and Q. Shafi, *Nucl. Phys.* **B 346** (1990) 193.
- [42] L. Visinelli and P. Gondolo, *Phys. Rev.* **D 81** (2010) 063508.
- [43] L. Duffy *et al.*, *Phys. Rev. Lett.* **95** (2005) 091304 and *Phys. Rev.* **D 74** (2006) 012006; for a review, see S. Asztalos, L. Rosenberg, K. van Bibber, P. Sikivie and K. Zioutas, *Ann. Rev. Nucl. Part. Sci.* **56** (2006) 293.